JOURNAL OF
MECHANICAL ENGINEERING

The Institution of Engineers, Bangladesh
Volume: ME 53, No. 1, December 2023

MECHANICAL ENGINEERING DIVISION

ISSN: 0379-4318

JOURNAL OF
MECHANICAL ENGINEERING

Volume: ME 53, No. 1, December 2023

Published by :

MECHANICAL ENGINEERING DIVISION
The Institution of Engineers, Bangladesh
Head Quarters : Ramna, Dhaka-1000
Bangladesh

JOURNAL OF
MECHANICAL ENGINEERING
Volume: ME 53, No. 1, December 2023

EDITORIAL BOARD

CONTENTS :

TOOL WEAR MONITORING WITH VIBRATION SIGNAL USING RECURRENT NEURAL NETWORK IN TURNING OPERATION OF HARDENED STEEL

Aquib Rahman[1], Md. Tanvir Ahmed, Jannatul Fatima Kabir, Shah Md. Ashiquzzaman Nipu, Tahmid Akter
Department of Mechanical and Production Engineering (MPE)
Ahsanullah University of Science and Technology (AUST), Tejgaon Industrial Area, Bangladesh
Corresponding Email: aquib.rahman.mpe@aust.edu

Abstract: *The primary goal of primary goal is to try to predict the time needed for targeted tool wear using a recurrent neural network model. Unlike other Neural Networks, it is able to recognize the pattern and as a result, this neural network is prodigious for sequential data. The data used in this experiment is identified as time series data. The turning operation was done with a coated carbide cutting tool on the material (52 HRC). The accelerometer was used for capturing the vibration data from machining and the data was then transferred to the computer for processing. The tool wear of the cutting tool was determined using the metallurgical microscope. After that, the vibration data was fed into the model, and the developed Recurrent Neural Network (RNN) model was able to predict the time for the tool wear that takes place in the cutting tool. Generally, gradual tool wear takes place in coated carbide before tool failure which can be predicted through this model. And due to this fact, it was possible to predict the time required for a targeted tool wear value.*

Keywords: *RNN; Machine Learning; Vibration; Carbide Tool; Hardened Steel, Taguchi*

INTRODUCTION

Monitoring tool wear is one of the challenging tasks associated with monitoring tool conditioning for the machining process. Changing the tools automatically due to tool wear or disfigurement is a big challenge for manufacturing industries and nearly 7% downtime of machines take place due to tool failure [1]. This wear is the result of physical phenomena that occur during cutting, mainly friction. By observing the strength of this phenomenon, it is possible to conclude indirectly the expansion of cutting wear. There are two types of tool condition monitoring, and they are indirect & direct [2]**.** The most commonly used phenomenon for monitoring the condition of cutting edges, such as power (force), vibration, sound, temperature, and timing. Based on these signals, it is possible to elicit the relevant characteristics and determine the status of the instrument. Recent developments in machine tools, computerized control, and automatization, combined with the related unforeseen improvements in the cutting materials and their protective coatings with special geometrical shapes of the tools [3]. The material used in this experiment was ferritic steel with HRC 48-52 & the cutting tool used in this experiment was coated carbide. The ferritic steel with HRC 48-52 was selected because the coated carbide has high hardness & good heat resistance. As the cutting tools have high hardness & good heat resistance, the steel with high hardness was selected. Since the work material was a shaft, the turning operation was performed on the work because the lathe machine is able to give high precision when it comes to machining round shapes. Tool life can also be predicted through the use of machine learning. Due to the rarity of system behavior for complex processes & systems of manufacturing, Data driven methods are often used to build models. There are two types of categories in prognostics, and they are model based & data-based [4]**.** This experiment uses Recurrent Neural Network by using the vibration data, time frame & tool wear from the experimental values to predict the tool wear that takes place in the principal flank face of the cutting tool. Flank & crater wear are the two principal types of tool wear that takes place because of these activities. But the industry only takes flank wear as a variable because its effectiveness is linked [5]. This model was used because model almost gave good precision in predicting the tool wear. With the experimental data, the model was close to perfect in predicting the tool wear. With the help of three machining parameters cutting speed, feed rate & depth of cut. Several studies are conducted to determine the relationship between cutting forces and parameters. When employing CBN tools, the depth of the cut was found to be the parameter that had the greatest impact on the cutting forces [6]. Furthermore, cutting speed has a disproportionately large impact on tool wear when it comes to PVD-coated (Ti CN) ceramic tools, where abrasion is the primary cause of tool wear [7]. Rather than the depth of cut and cutting speed, feed rate also has a significant impact on surface roughness. It is advised to use a lower feed rate while finishing hardened steel. Tool wear is a very crucial part of manufacturing industries. As tool wear leads to tool failure. There's been a correlation between tool wear and tool life. When tool wear takes place, it releases vibration waves. The conventional way of determining tool wear is a costly process. Many researchers have overlooked this topic. The purpose of this experiment will be to try and detect the tool wear of a cutting tool for determining the tool failure in the lathe machine by setting up an accelerometer sensor and processing the acquired data using an Arduino Uno board. This way the process of

determining tool wear will become cheaper and it can affect manufacturing in many ways.

METHODOLOGY

At first, the hardness of the material was increased from 34 HRC(Average) to 48-52 HRC. For machining, the described material, cutting tools & tool holders were selected. Each edge of the cutting tool was used in this experiment for observing the tool failure. All of the parts have been a perfect fit with one another to ensure the data is reliable and for the purpose of repeatability of the experiment.

Cutting tool specifications:

The table below gives the cutting tool details which were used in this research.

Table 1: Cutting tool specifications

Insert Shape:	Square, 90 degrees
Insert Clearance Angle:	0 degree
Type of Insert:	With hole and Chip breaker
Tool:	Coated Carbide
Manufacturer:	RUIAN
Metric:	SNMG120404-GM
Grade:	MC7025
Composition:	Al_2O_3 + TiC

Table 2 contains the cutting tool properties at different conditions and important properties associated with the experiment:

Table 2: Cutting tool properties

Room temperature hardness:	1900 HV
Hardness at 1000 ^{0}C:	800 HV
Fracture toughness:	3.3 MPa $m^{1/2}$
Thermal conductivity:	12 – 18 W/m^{0}C
Young's Modulus:	420 kN/mm^2
Coefficient of thermal expansion:	8×106/K

The experiment used ferric steel as the workpiece. The detail of the workpiece is given in table 3. Furthermore, the workpiece was hardened to achieve the desired hardness. Table 4 contains the chemical composition of the selected workpiece.

Table 3: Work material details

Name:	Ferric Steel
Type:	Shaft
Diameter:	62 mm
Hardness (Rockwell):	48-52 HRC
Length:	304.8 mm

Table 4: Chemical composition of work specimen

C (wt.%)	Si (wt.%)	Mn (wt.%)	P (wt.%)	S (wt.%)
0.17	0.17	0.87	0.011	0.013

Machine Specifications:

The lathe machine is said to be the mother of all machines as it is probably the oldest machine used extensively in manufacturing industries. They are three jaws & four Jaws. The model name of the High-Speed Engine Lathe is CB6266B. The manufacturer's name is MOCHA. This lathe machine can perform taper turning, and external & internal turning. It's a horizontal lathe machine. The setting mode is floor type.

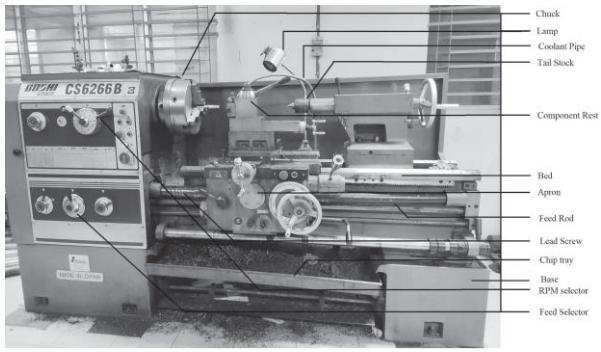

Figure 1: Mocha CS6266B Lathe Machine

Cutting Conditions:

The cutting operation was conducted in a dry condition which means any types of lubricants & coolants were not used as it was our desired experimental requirement. Since the tool was coated, the coating worked as a solid lubricant which reduced friction & adhesion.

Sensor specification:

The accelerometer sensor was used to capture the vibration that gets generated during the machining. This accelerometer is able to generate 3-Axis (X, Y, Z) data. Table 5 explains the properties of the sensor used to collect vibration data during the machining of the hardened steel specimen.

Table 5: Sensor properties

Name:	ADXL345
Measurement Range:	± 2, ± 4, ±8, ±16 g

Device weight:	30mg
Operating Temperature Range:	-40° to +80° C

Arduino Specification:
The Arduino Uno was used to collect the data from the accelerometer. The Arduino was programmed to capture continuous data with C++ using the open-source software Arduino IDE. The Arduino board was connected to the computer with the help of a USB cable.

Table 6: Arduino Uno details

Micro-controller:	ATmega328
Voltage:	5V
Digital input and output:	14
SRAM	2KB

Code used in Arduino Uno for data collection:

```
#include <Wire.h> int ADXL345 = 0x53; int X_out, Y_out, Z_out; void setup() {
Serial.begin(9600);
Wire.begin();
Wire.beginTransmission(ADXL345);
Wire.write(0x2D);
Wire.write(8); Wire.endTransmission(); delay(10); }
void loop() {
Wire.beginTransmission(ADXL345);
Wire.write(0x32);
Wire.endTransmission(false);
Wire.requestFrom(ADXL345, 6, true);
X_out = ( Wire.read() | Wire.read() << 8);
Y_out = ( Wire.read() | Wire.read() << 8);
Z_out = ( Wire.read() | Wire.read() << 8);
Serial.print(X_out);
Serial.print(" ");
Serial.print(Y_out);
Serial.print(" "); Serial.println(Z_out); delay(100);
```

The amount of tool wear that occurred in coated carbide tools while cutting hardened steel was observed using a microscope (Inverted metallurgical microscope). Ceramic tools generally lack durability and are fragile by nature. resulting in rapid tool life degradation from wear, including material diffusion into the cutting tool and chipping of the rake face and primary flank. To say the least, these are some significant wears. Its hardness makes some really difficult machining possible. The tool maker's microscope was able to narrow in on the exact location of the tool wear as well as how much vertical or horizontal tool wear developed during the machining process. The disadvantage of this procedure is that the specimen must have a very small size. This method also has the drawback of some light elements going undetected and the observation of wear depth being frequently erroneous.

Design of Experiment
DOE helps find the optimized result minimizing the time & cost while maximizing accuracy. The test run amount was limited. The trend of the overall population of data can be found with a very limited sample. In turning operation, there are a lot of factors that can be taken into account for machining parameters. However, a survey of the literature reveals that the most important input parameters taken into account by the researchers were the depth of cut (d, mm), cutting speed (v, m/min), and feed rate (f, mm/rev).

While other parameters were expected to remain constant throughout the experiment, these were chosen as design elements for the current investigation. In this experiment, 9 experimental runs in total have been considered.

To reduce the inaccuracy caused by the machining setup, an experimental run using randomization has been performed. Table 3.3.2 lists the levels of cutting parameters, such as depth of cut, cutting speed, and feed rate, for the tests that were carried out in accordance with the experimental plan based on the Taguchi L9 technique. The experimental plan based on a central composite face-centered design has been followed in the execution of the experiments. The experiment run order and standard order are both parts of the experimental plan, coded values for the process parameters and observed responses are displayed in the Table below:

Table 7: Response Tool Wear Design: Factors

Factors	Name	Low	High
A	Cutting Speed	100 m/min	200 m/min
B	Feed	0.1 mm/rev	0.16 mm/rev
C	Depth of Cut	0.2 mm	0.40 mm

Table 8: Taguchi L9 Design: Design Summary

Factors:	3	Replicates:	1
Base runs:	9	Total Runs	9
Base blocks:	1	Total Blocks:	1

Table 9: Experimental results of cutting tool wear

Run	A (m/min)	B (mm/rev)	C (mm)	Avg. Flank Wear
1	100	0.1	0.2	231.25
2	100	0.13	0.35	159.38
3	100	0.16	0.5	275
4	150	0.1	0.35	262.5
5	150	0.13	0.5	256.25
6	150	0.16	0.2	287.5
7	200	0.1	0.5	221.88
8	200	0.13	0.2	259.38
9	200	0.16	0.35	287.5

Recurrent Neural Network

The Data acquired from the Accelerometer were Time series data because it generated X-axis, Y-axis & Z-axis values from the vibration with respect to time. This type of data performs well with Recurrent Neural Networks. At first, the data was saved into separate comma-separated value(.CSV) files, and then from there, it was loaded into the google co-lab IDE with the help of python's library pandas as a datagram. Data frame helps to organize and manage data more easily. Then the data was separated into three parts. They are train data, test data & validation data. and the ratio for separating these data was 70% train data, 20% validation data & 10% test data. Normally machine learning models require train & test data but building neural networks requires validation data since the neural networks can optimize themselves. After that, the model was built with python's machine learning framework TensorFlow. One layer of LSTM(Long Short-Time Memory) was used to process the data. The recursive option was activated so that the model can call itself from inside the function all by itself.

Model Formulation:

The vibration data along with time & tool wear were useful for building the model because these values are responsible for recognizing the pattern. Recurrent neural networks are basically networks with loops in them, thus allowing information to persist. A normal neural network doesn't have the capability to persist its data. RNN can be thought of as multiple copies of the same network. Because of the chain-like structure, the RNN is able to work with sequential data. The data used in this experiment was Time series data. And RNN models work appropriately with time series datasets.

The RNN model used for this experiment is:

$$f_t = \sigma\,(W_t.[h_{t-1}, x_t] + b_f) \quad (1)$$

$$\text{Here, } it = \sigma\,(Wi.[ht\text{-}1, xt] + bi) \quad (2)$$

$$\acute{C}_t = \tanh(W_c.\,[h_{t-1}, x_t] + b_c) \quad (3)$$

$$Ct = ft * Ct\text{-}1 + it * \acute{C}t\ \sigma \quad (4)$$

$$o_t = \sigma\,(W_o\,[h_{t-1}, x_t] + b_o) \quad (5)$$

$$ht = ot * \tanh(Ct) \quad (6)$$

Here,

$\acute{C}_t$ = candidate for cell state at timestamp
c_t = Cell state
b = biases for the respective gates
w= Weights for the respective gate
O_t = Output gate
i^t = Input gate

RESULTS AND DISCUSSION

For determining the tool wear of the cutting tool for each run the Inverted metallurgical microscope was used. Through the microscope software average principal flank wear was determined. Following are the condition of the tool that was observed after the run with 0.5 mm depth of cut, 100 m/min cutting speed, and 0.16 mm/rev. With the microscope interface the height, area, and width of the used tool were determined which indicates at what period the tool failed. Figure 2 shows the 10X zoom photo of tool wear in explained conditions.

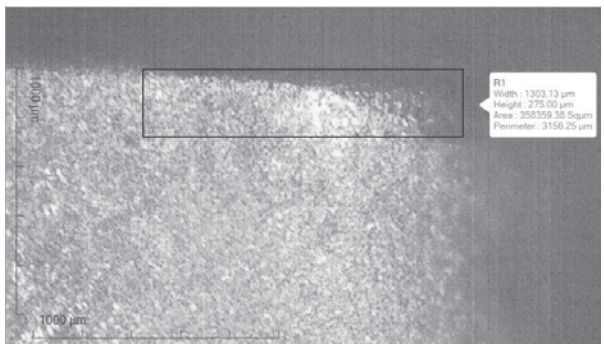

Figure 2: Microscopic image of tool wear (H: 275µm, W:1303.3µm, and A:358359.38Sqµm)

During machining, the sensor and Arduino uno setup was connected to the machine and computer where during machining the sensor captured vibration data in 3 different axes. After acquiring vibration data in three axes, raw data were plotted against time to visualize the data changes in X, Y, and Z axis. As accelerometer data also compromise gravitational data, it was removed from the axis to acquire an appropriate representation of datasets. Figure 3 shows the initial vibration data in three different axes.

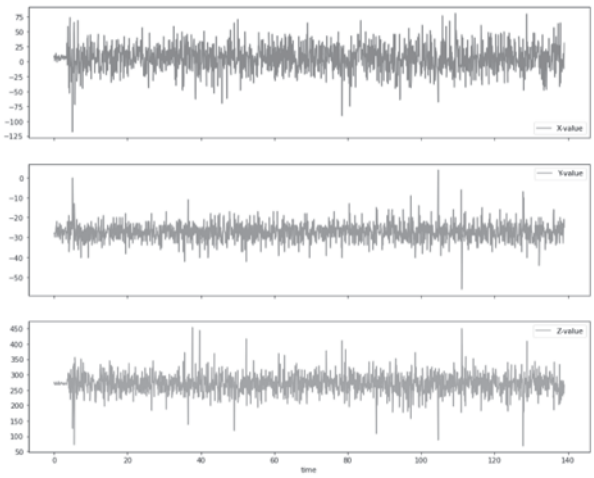

Figure 3: Vibration data of the X-axis, Y-axis & Z-axis with respect to time.

The graphs were plotted with the use of Python's visualization library Matplotlib. For the initial run, at first, the data was normalized because it helps the model to calculate easily and learn faster. After that, the data was fed into the model and after 10 epochs the loss & validation loss value was found to be 2.7607e-04 and 4.7346e-04. And the graph was plotted using the actual value & predicted value and in figure 4.

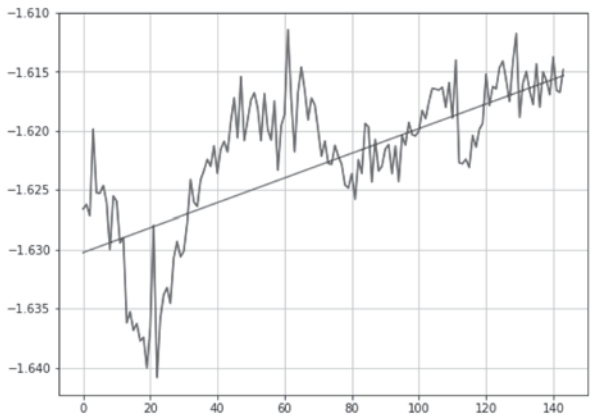

Figure 4: Graph plotted with the normalized data of the vibration, time & tool wear.

It is shown that the model was accurately able to predict the test data. And since the model can accurately predict the tool wear which is 275µm. It can be said that This model can predict when the tool wear will reach 0.3µm, which is the tool failure point.

After comparing the calculated value and observed value it was found that the model is capable of monitoring tool conditions with given specifications and predicting the time for tool failure.

CONCLUSION

In this research work, following the design of the experiment, the experiment was conducted with coated carbide tool in the machining of hardened steel. Coated carbide tools have good heat resistance because The covering substance resists heat well. It has high hardness compared to carbide inserts that are ordinary. It has higher tool life. The Taguchi L9 was selected for the optimized experiment instead of doing all possible experiments. The task at hand entails calculating the typical tool wear of the main flank area. The objective of this experiment was to try to predict the time it will take for reaching the targeted tool wear of the cutting tool using the vibration & timeframe. The data taken from the experiment was used to fit the Recurrent Neural Network model. At first, the data was prepared using python. Then the data was Normalized for feeding the model easily. After that, the data was fed into the Recurrent Neural Network algorithm which gave a loss score of 2.7607e-04 & validation loss of 4.734e-04 which means the model is almost accurate. That means this model can predict the time required for the gradual tool wear to reach the failing point which is 0.3µm after providing the model vibration data along with tool wear & time frame. There are some recommendations for future research:

1. It is possible to predict more accurate data by using more data.
2. It is possible to build different machine-learning models using experimental data.
3. Independent variables can be varied and then used to build different models for different investigation approaches.

NOMENCLATURE

RNN= Recurrent Neural Network
CBN=Cubic Boron Nitride
$\acute{C}_t$ = candidate for cell state at timestamp
c_t = Cell state
b = biases for the respective gates
w= Weights for the respective gate
O_t = Output gate
i^t = Input gate

REFERENCES

[1] G. Vetrichelvan, S. Sundaram, S. Senthil Kumaran, and P. Velmurugan, "An investigation of tool wear using acoustic emission and genetic algorithm," *JVC/Journal Vib. Control*, vol. 21, no. 15, pp. 3061–3066, 2015.

[2] P. Twardowski, M. Tabaszewski, M. Wiciak – Pikuła, and A. Felusiak-Czyryca, "Identification of tool wear using acoustic emission signal and machine learning methods," *Precis. Eng.*, vol. 72, no. December 2020, pp. 738–744, 2021.

[3] X. Li, "A brief review: Acoustic emission method for tool wear monitoring during turning," *Int. J. Mach. Tools Manuf.*, vol. 42, no. 2, pp. 157–165, 2002.

[4] T. Mikołajczyk, K. Nowicki, A. Bustillo, and D. Y. Pimenov, "Predicting tool life in turning operations using neural networks and image processing," *Mech. Syst. Signal Process.*, vol. 104, pp. 503–513, 2018.

[5] J. L. Ferrando Chacón, T. Fernández de Barrena, A. García, M. Sáez de Buruaga, X. Badiola, and J. Vicente, "A Novel Machine Learning-Based Methodology for Tool Wear Prediction Using Acoustic Emission Signals," *Sensors (Basel).*, vol. 21, no. 17, pp. 1–16, 2021.

[6] G. Bartarya and S. K. Choudhury, "Influence of machining parameters on forces and surface roughness during finish hard turning of EN 31 steel," *Proc. Inst. Mech. Eng. Part B J. Eng. Manuf.*, vol. 228, no. 9, pp. 1068–1080, 2014.

[7] R. Suresh and S. Basavarajappa, "Effect of Process Parameters on Tool Wear and Surface Roughness during Turning of Hardened Steel with Coated Ceramic Tool," *Procedia Mater. Sci.*, vol. 5, pp. 1450–1459, 2014.

FUNDAMENTAL OF FINITE ELEMENT ANALYSIS (FEA) AND SOLVING STIFFNESS MATRIX BY NEWTON-RAPHSON METHOD

Fazlar Rahman[*1] and Mohammad Sarwar Morshed[1]

[1]Faculty, Department of Mechanical and Production Engineering (MPE)
Ahsanullah University of Science and Technology (AUST), Dhaka, Bangladesh

[*]Corresponding Author Email: fazlar.rahman.mpe@aust.edu; fazlar19@hotmail.com

Abstract: *Finite Element Analysis (FEA) is the most popular technique used to solve a wide range of complex engineering problems and physical phenomena without prototypes. It allows simulating real-world boundary value problems for feasibility study, design, optimization, better understanding, and prediction without lab environments. It is an efficient and cost-effective numerical technique useful to simulate structural, thermo-fluid environment, vibration, wave propagation, biomechanical, contact analysis, and other phenomena with complex geometry, indeterminate and non-ideal boundary conditions, nonlinear load, and material properties where an analytical solution is difficult. In FEA, physical systems are divided into a number of small segments or elements connected by a number of grids/nodes. Depending on the discretization of the system, each element will have at least two nodes, some degrees of freedoms (DOFs), and resistance to deform and be displaced under load, called element stiffness. The stiffness matrix of each element is determined from the integral or weak form of the differential equation, which governs the element's behavior based on boundary value. The stiffness matrix for each element is assembled to form the stiffness matrix of the entire structure/system, called the global stiffness matrix, which represents the resistance of the entire system to deformation under load. The strain/stress at nodes of the discretized system are determined from the solution of the global stiffness matrix. The analytical solution of the global stiffness matrix is difficult and inefficient depending on the size of the system and the number of discrete elements. The numerical analysis tools, such as ANSYS, ABAQUS, IDEAS, FEAMAP, COSMOS, Natran/Patran, MatLab, etc., are available to solve the global stiffness matrix. However, without knowing the fundamentals of FEA and the technique used to solve the global stiffness matrix behind the FEA tools, it is challenging to achieve the solution and accuracy. This study provides the fundamentals of finite element analysis (FEA) and solving stiffness matrixes by the Newton-Raphson method, which will help users achieve the accuracy of the FEA solution.*

Keywords: *Finite Element Analysis; Simulation, Stiffness matrix; Newton-Raphson method, Numerical analysis.*

INTRODUCTION

Finite Element Method (FEM) is a numerical technique used to solve a wide range of engineering problems and physics, where a physical system is divided into numbers of small segments or elements connected by grids or nodes. When FEM is applied to solve a complex engineering problem and physics, it is called finite element analysis (FEA) [1]. It offers the appropriate solution to boundary value problems [2]. Boundary value problems are also known as field problems, where a physical structure or interested domain is called a field [1]. One or more dependent or field variables must satisfy the differential equation within a known domain of independent variables and specific conditions at the boundary [3]. The field variables include displacement, twisting, temperature, heat flux, fluid velocity, etc. [1]. The FEA is useful to solve problems with irregular and complex geometry, indeterminate structures, non-ideal boundary conditions, loads, geometry, and material properties, where an analytical solution is difficult. It is the most popular technique used to solve a wide range of complex engineering problems and physical phenomena without prototypes. It allows simulating real-world boundary value problems for feasibility study, design, optimization, better understanding, and prediction without lab environments [1]. It is an efficient and cost-effective numerical technique useful to simulate structural, thermo-fluid environment, vibration, wave propagation, biomechanical, contact analysis, and other phenomena with complex geometry, indeterminate and non-ideal boundary conditions, nonlinear load, and material properties where an analytical solution is difficult.

In FEA, physical systems are divided into a number of small segments or elements connected by a number of grids or nodes. Depending on the discretization of the system, each element will have at least two nodes, some degrees of freedom (DOFs), and resistance to deform or be displaced under load, called element stiffness. The

stiffness matrix of each element is determined from the integral or weak form of the differential equation, which governs the element's behavior based on boundary conditions or boundary value [3]. The stiffness matrix for each element is assembled to form the stiffness matrix of the entire structure or system, called the global stiffness matrix, which represents the resistance of the entire system to deformation under load [1, 4]. The displacement, deformation, and strain at nodes of the discretized system are determined from the solution of the global stiffness matrix. However, the analytical solution of the global stiffness matrix is difficult and inefficient, depending on the size of the system and the number of discrete elements. Due to the intense development of the computation capacity of personal computers, various numerical analysis tools, such as ANSYS, ABAQUS, IDEAS, FEAMAP, COSMOS, Natran/Patran, MatLab, etc., are available commercially to solve the global stiffness matrix. It is challenging to achieve the solution of the stiffness matrix with suitable accuracy without knowing the fundamentals of FEA and the technique used to solve the global stiffness matrix behind the FEA tools. The commercially available FEA tools are widely used in the aerospace, defense, biomedical engineering, automobile industries, structural, thermo-fluid interface, heat transfer, vibration, and contact analysis, as well as validation of experimental studies and design optimization [1-6]. This study provides the fundamentals of finite element analysis (FEA) and solving stiffness matrixes by the Newton-Raphson method, which will help users achieve the appropriate accuracy of the FEA solution and a better understanding of the features behind the FEA tools. Since the accuracy of the FEA solution is crucial for its the acceptability, reliability, and validity [7].

METHODOLOGY

Development of stiffness matrix:

Based on the discretization method, each element of the physical system or structure will have at least two nodes, degrees of freedom (DOFs), and resistance to deform and displace under load, which is called element stiffness or spring constant. It represents how element nodes will be displaced and deformed under load. This behavior of the element can be represented by equation (1) [3].

$$\{f\} = [k]\{u\} \tag{1}$$

where, {f} is the force vector acting on each node of the element, {u} is the displacement vector of each node, and [k] is the stiffness matrix of the element. The displacement vector {u} depends on the type of element and nodal force vector.

Degrees of freedom of a 2D beam element is shown in **Fig.-1** [4].

Fig.-1: 2D Beam Element with three degrees of freedom.

The displacement vector of nodes and the standard stiffness matrix of the 2D beam element are shown below [4]. The stiffness matrix includes axial, bending, and rotational stiffness.

$$\{u\} = \begin{Bmatrix} u_1 \\ v_1 \\ \theta_1 \\ u_2 \\ v_2 \\ \theta_2 \end{Bmatrix} \tag{2}$$

and

$$[k] = \begin{bmatrix} \frac{AE}{L} & 0 & 0 & -\frac{AE}{L} & 0 & 0 \\ 0 & \frac{12EI}{L^3} & \frac{6EI}{L^2} & 0 & -\frac{12EI}{L^3} & \frac{6EI}{L^2} \\ 0 & \frac{6EI}{L^2} & \frac{4EI}{L} & 0 & -\frac{6EI}{L^2} & \frac{2EI}{L} \\ -\frac{AE}{L} & 0 & 0 & \frac{AE}{L} & 0 & 0 \\ 0 & -\frac{12EI}{L^3} & -\frac{6EI}{L^2} & 0 & \frac{12EI}{L^3} & -\frac{6EI}{L^2} \\ 0 & \frac{6EI}{L^2} & \frac{2EI}{L} & 0 & -\frac{6EI}{L^2} & \frac{4EI}{L} \end{bmatrix} \tag{3}$$

The stiffness matrix of the beam element is derived from the solution of the following differential equation (4) [4].

$$EI\frac{d^4v(x)}{dx^4} = q(x) \tag{4}$$

The stiffness matrix [k] depends on the element type, geometry, and material properties. The stiffness matrix of each element is determined from the integral or weak form of the differential equation (4), which governs the element's behaviour. Two methods, such as the Principle of Minimum Potential Energy and Galerkin Weighted Residual Methods, are used to derive and solve the weak form of the differential equation (6) using the property values at boundaries [1, 3]. However, the Galerkin weighted residual method is the most popular [2].

Once the stiffness matrix for each element of the discretizing structure is developed, they are assembled to form the stiffness matrix of the entire structure, which is known as the Global stiffness matrix [1]. It represents

the resistance to the deformation of the whole structure. The behavior of the entire structure is governed by equation (5).

$$\{F\} = [K]\{U\} \quad (5)$$

where {F} is known and represents the force vector of all nodes of the discretized or meshed structure. The vector {U} is unknown, which indicates the displacement and rotation of nodes, and $[K]$ is the Global stiffness matrix. The strain and stress at each node of the discretized structure are determined by the displacement and rotation of nodes, which are obtained by solving equation (6).

$$\{U\} = [K]^{-1}\{F\} \quad (6)$$

Depending on the size and mesh density, it is difficult and inefficient to solve equation (6) analytically. Some numerical analysis tools, such as ANSYS, ABAQUS, IDEAS, FEAMAP, COSMOS, Natran/Patran, MatLab, etc., are available to solve the stiffness matrix or equation (6). For evaluating the value of a variable within the element, the shape or blending function is used, which interpolates the nodal value of a property at any location within the element [2]. For example, the field variable of a 2D triangular element can be evaluated using the following shape function [1], as shown in equation (7).

$$\varphi(x,y) = N_1(x,y)\varphi_1 + N_2(x,y)\varphi_2 + N_3(x,y)\varphi_3 \quad (7)$$

where φ_1, φ_2, and φ_3 are values of the field variable at three nodes of the element, and N_1, N_2, and N_3 are the interpolation functions. The shape function depends on the element type, number of nodes and field variables, and degrees of freedom. The element with a higher number of nodes or mid-nodes will provide higher accuracy in evaluating field variables within the element. The Newton-Raphson method is the most popular to solve the Global stiffness matrix in the FEA tool.

Newton-Raphson method:

The Newton-Raphson method can be used to solve the root of a single variable function and system of nonlinear functions.

Root of single variable function

The Newton-Raphson method is used to approximate the root of a continuous, differentiable, and real-valued function, f(x) = 0. It implements the concept of approximation of the root of a function by a straight line tangent [8], as shown in **Fig.-2**. It requires successive approximations to predict the root of the function. It has the advantage of quick estimation of the root of a function whose derivative exists.

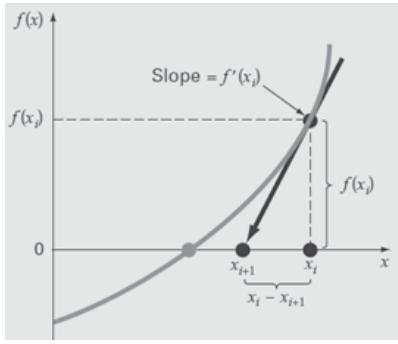

Fig.-2: Graphical presentation of Newton-Raphson method [8].

The slope of the function at x is equivalent to its first derivative.

$$f'(x_i) = \frac{f(x_i)}{x_i - x_{i+1}} \quad (8)$$

Rearranging equation (8) yield,

$$x_{i+1} = x_i - \frac{f(x_i)}{f'(x_i)} \quad (9)$$

where, X_i= Value of root at iteration i, X_{i+1} = Revised value of root at iteration i+1, $f(x_i)$ = Value of function at iteration i, and $f'(x_i)$ = Derivative of function f(x) evaluated at iteration i.

A repeated approximation is needed to find the root of a real value function within the tolerance limit. The solution fails to converge if $f'(x_i)=0$. In the convergence of the Newton-Raphson method, the following condition has to be satisfied [9].

$$|f(x_i) \cdot f''(x_i)| < |f'(x_i)|^2 \quad (10)$$

The initial estimate has to satisfy the condition mentioned in equation (10) for convergence of the solution. The approximation error can be evaluated using equation (11) [8].

$$|\epsilon_a| = \left|\frac{x_{i+1} - x_i}{x_{i+1}}\right| \times 100 \quad (11)$$

The general form of the Newton-Raphson method, equation (9) can be used to find the root of a nonlinear equation with a single variable.

Roots of system of nonlinear functions

The general form of the Newton-Raphson method has to be modified to find the roots of a system of

nonlinear equations. A system of nonlinear equations can be written in vector form, as shown below.

$$\mathbf{f(x)} = 0 \tag{12}$$

where, $\boldsymbol{x} = \begin{pmatrix} x_1 \\ x_2 \\ . \\ . \\ . \\ x_n \end{pmatrix}$ and

$$\begin{pmatrix} \boldsymbol{f}_1(x_1, x_2, \dots, x_n) \\ \boldsymbol{f_2}(x_1, x_2, \dots, x_n) \\ . \\ . \\ . \\ \boldsymbol{f_n}(x_1, x_2, \dots, x_n) \end{pmatrix} = \begin{pmatrix} 0 \\ 0 \\ . \\ . \\ . \\ 0 \end{pmatrix} \tag{13}$$

The general form of the Newton-Raphson method can be modified by incorporating the Jacobian matrix, **J** in equation (9), which contains partial derivatives of **f**(**x**) [10].

$$\mathbf{x}_{i+1} = \mathbf{x}_i - \frac{\mathbf{f}(x_i)}{\mathbf{J}(\mathbf{x})} \tag{14}$$

where, $\mathbf{J}(\mathbf{x}) = \begin{bmatrix} \frac{\partial f_1}{\partial x_1} & \frac{\partial f_1}{\partial x_2} & \dots & \frac{\partial f_1}{\partial x_n} \\ \frac{\partial f_1}{\partial x_1} & \frac{\partial f_1}{\partial x_2} & \dots & \frac{\partial f_1}{\partial x_n} \\ . & . & \dots & . \\ . & . & \dots & . \\ \frac{\partial f_n}{\partial x_1} & \frac{\partial f_n}{\partial x_2} & \dots & \frac{\partial f_n}{\partial x_n} \end{bmatrix}$ (15)

Equation (14) can be reformed for a system of equation **f**(**x**) = 0, as shown below,

$$\mathbf{x}^{(\alpha)} = \mathbf{x}^{(\alpha-1)} - \mathbf{J}^{-1}\left(\mathbf{x}^{(\alpha-1)}\right) \cdot \mathbf{f}\left(\mathbf{x}^{(\alpha-1)}\right) \tag{16}$$

where, α is the number of iteration, i.e. α = 1, 2, 3, …, n. Equation (16) can be rearrange as,

$$\mathbf{J}\left(\mathbf{x}^{(\alpha-1)}\right) \cdot \left(\mathbf{x}^{(\alpha)} - \mathbf{x}^{(\alpha-1)}\right) = -\mathbf{f}\left(\mathbf{x}^{(\alpha-1)}\right) \tag{17}$$

$$\mathbf{J}\left(\mathbf{x}^{(\alpha-1)}\right) \cdot \boldsymbol{\delta x}^{(\alpha-1)} = -\mathbf{f}\left(\mathbf{x}^{(\boldsymbol{\alpha-1})}\right) \tag{18}$$

where, $\boldsymbol{\delta x}^{(\alpha-1)} = \mathbf{x}^{(\alpha)} - \mathbf{x}^{(\alpha-1)}$. Arranging equation (18) yields,

$$\boldsymbol{\delta x}^{(\boldsymbol{\alpha-1})} = -\boldsymbol{J}^{-1}\left(\boldsymbol{x}^{(\boldsymbol{\alpha-1})}\right) \cdot \boldsymbol{f}\left(\boldsymbol{x}^{(\boldsymbol{\alpha-1})}\right) \tag{19}$$

Substituting the value of $\boldsymbol{\delta x}^{(\boldsymbol{\alpha-1})}$ from equation (19) to equation (16),

$$\mathbf{x}^{(\alpha)} = \mathbf{x}^{(\alpha-1)} + \boldsymbol{\delta x}^{(\boldsymbol{\alpha-1})} \tag{20}$$

For a given initial vector,

$\mathbf{x}^{(0)} = \begin{pmatrix} \mathbf{x}_1^{(0)} \\ \mathbf{x}_2^{(0)} \\ . \\ . \\ \mathbf{x}_n^{(0)} \end{pmatrix}$, the first iteration can be found from the equation (20).

$$\mathbf{x}^{(1)} = \mathbf{x}^{(0)} + \boldsymbol{\delta x}^{(\mathbf{0})}$$

$$\mathbf{x}^{(2)} = \mathbf{x}^{(1)} + \boldsymbol{\delta x}^{(\mathbf{1})}$$

$$\mathbf{x}^{(3)} = \mathbf{x}^{(2)} + \boldsymbol{\delta x}^{(\mathbf{2})} \text{ and so on.}$$

The process is repeated until solutions of **f**(**x**) = 0 reach within the acceptable limit. The numerical analysis (FEA) tools, such as ANSYS, IDEAS, MEMAP, NASTRAN, etc., use the Newton-Raphson method to solve the system of nonlinear equations of the stiffness matrix, {F}=[K]{U}.

Steps in Finite Element Analysis (FEA):

The following steps need to be followed to solve engineering problems and physics with FEA tools, as shown in **Fig.-3**.

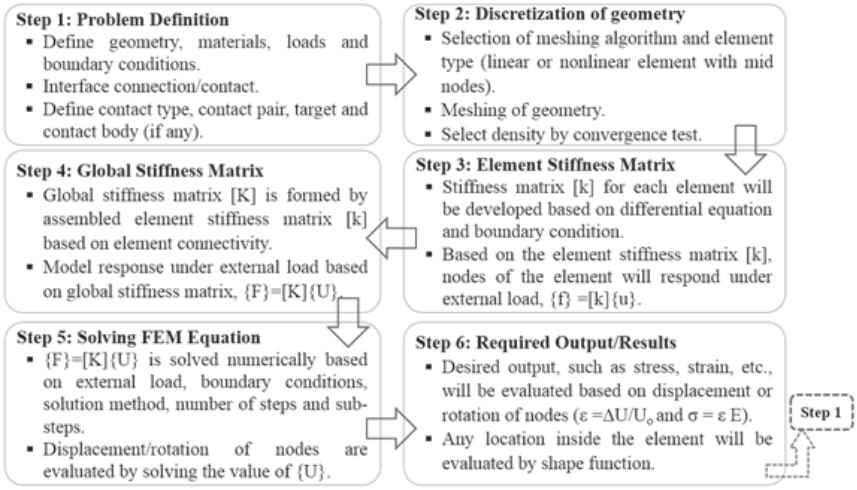

Fig.-3: Steps of Finite Element Analysis (FEA).

The user performs some steps, and some are completed by the FEA tool automatically. Steps 1, 2, 6, and part of Step 5 (solution method, number of steps, and sub-steps) must be performed by the user appropriately. Depending on the nature of physics and engineering problems, geometry, load, boundary conditions, and nonlinearity, the user has to discretize the physical systems and structures by implementing appropriate methods and element types.

CONCLUSIONS:

Finite Element Analysis (FEA) tools, such as ANSYS, ABAQUS, IDEAS, FEAMAP, COSMOS, Natran/Patran, MatLab, etc., are commercially available to solve complex engineering problems and physics. Most of them are user-friendly and built with a graphical user interface (GUI). However, without knowing the fundamentals and steps of finite element analysis (FEA) and the technique used to solve the global stiffness matrix behind the tools, it is challenging to achieve the FEA solution with appropriate accuracy and a cost-effective run time. This study provides the fundamentals of FEA and solving stiffness matrixes by the Newton-Raphson method, which will help users achieve the accuracy of the FEA solution. It will enrich the user's skills and knowledge about FEA tools and effective ways of solving engineering problems.

ACKNOWLEDGEMENT

The authors would like to acknowledge the Ahsanullah University of Science and Technology (AUST), Dhaka, Bangladesh.

REFERENCES:

[1] Hutton, D. V.; 2004, "Fundamentals of Finite Element Analysis", 1st edition, McGraw-Hill.

[2] Seshu, P.; 2012, "Textbook of finite element analysis" PHI Learning Pvt., New Delhi.

[3] The Efficient Engineer; 2023, "Understanding the Finite Element Method", Available online: https://efficientengineer.com/finite-element-method/.

[4] Moaveni, S.; 2011, "Finite Element Analysis Theory and Application with ANSYS", 3rd edition, Pearson Educaiton, India.

[5] Geng, J. P.; Tan,K. B. C.; Liu, R. Liu; 2001, "Application of finite element analysis in implant dentistry: A review of the literature," *J. Prosthet. Dent.*, 85(6): 585–598.

[6] Ye, Y.; You, W.; Zhu, W.; Cui, J.; Chen, K.; Wang, D.; 2017, "The Applications of Finite Element Analysis in Proximal Humeral Fractures," Computational and Mathematical Methods in Medicine, 2017.

[7] Tekkaya, A. E.; Martins, P. A. F.; 2009, "Accuracy, reliability and validity of finite element analysis in metal forming: A user's perspective," Engineering Computations: International Journal for Computer Aided Engineering and Software, 26(8): 1026–1055.

[8] S. C. Chapra, S.C.; Canale, R. P.; 2015' "*Numerical Methods for Engineers"*, 6th ed. McGraw Hill.

[9] BYJU'S, 2003, "Newton Raphson method." Available online: https://byjus.com/maths/newton-raphson-method

[10] Jia, H.; 2018, "Newton-Raphson Method and Arithmetic Mean Newton's Method for Solving Systems of Nonlinear Equations," Lakehead University, Ontario, Canada.

Development and Implementation of an Atmospheric Water Generator for Water Sustainability

Shah Murtoza Morshed[1], Mohammad Jawadul Hoque Rohan[2], Mohammad Mynul Islam Mahin[3], MD Simran Sadid[4], Md Jawad Bin Rouf[5], Mohammad Morshed[6]

Department of Mechanical and Production Engineering,

Ahsanullah University of Science and Technology, 141 & 142, Love Road, Tejgaon Industrial Area, Dhaka-1208

Corresponding Author E-mail: murtoza.ipe@aust.edu

Abstract

The aspiration of this project was to design and fabricate a product addressing the problem of scarcity of water. Through extensive market research and testing, atmospheric water generator was the solution that was developed. The development process included CAD software for designing and 3D printing for rapid prototyping. The final product "Atmospheric Water Generator" is a device that generates water without relying on traditional water sources. This technology holds the potential to transform the way of getting access to water and more specifically, how people from water scarce area will have the access of drinkable water. This device works on the principle of condensation. It contains two basic process- dehumidification and filtration. The process of dehumidification involves cooling the air, causing the moisture in it to condense into water droplets. Then filtration is done to make it drinkable. Air to water converters use a variety of designs and technologies, but they all generally work on the same fundamental ideas. While some models utilize a desiccant to absorb moisture, others employ a refrigerant to chill the air. Typically, the extracted water is gathered in a tank or reservoir where it can be used for drinking or other uses. Developing an energy-efficient air to water converter is one of the biggest challenges. In many types, the cooling or drying operation is powered by electricity, which can be expensive in locations with scarce or expensive power. Some more recent designs power the device with sustainable energy sources, including solar panels, which can aid. Overall, an air to water conversion technology has the potential to revolutionize access to clean drinking water in challenging environments, including remote locations and disaster relief situations. Its implementation can greatly enhance the standard of living for individuals worldwide.

Keywords: *Atmospheric Water Generator, AWG, Filter, Water, Sustainable, Research Gaps*

1. Introduction

Due to population growth and contamination of the water that is available, particularly in water tables that provide water for general consumption, the global shortage of fresh water has increased exponentially (Mendoza-Escamilla et al., 2019). Even though 70% of our planet is covered in water, only 2.5% of it is freshwater. One-third of the world's population, according to a World Health Organization (WHO) study, lacks access to safe drinking water, and more than three billion people lack access to clean water for personal hygiene. In the context of the ongoing global battle against the coronavirus pandemic, people have recently come to realize how crucial it is to have access to clean water (Raveesh et al., 2021). The humane society is in danger of running out of fresh water. Climate change, urbanization, population growth, inadequate wastewater treatment, and synthetic pollutants entering the water system are all contributing to the depletion of freshwater resources. In a lot of places, the water crisis has already caused or will soon cause a food crisis. Water conservation, pollutant management from the polluting water cycle, infrastructure upgrade, and improved water generation technologies are some of the measures that must be

implemented to avoid the impended water–food crisis. As a result, in order to meet the growing demand, research and development into alternative sources of fresh water are unavoidable (Faraz Ahmad et al., 2022). Water production, reclaiming unused water, and a variety of water-saving strategies are the foundations of potential solutions to the problem of water scarcity. Reverse osmosis seawater desalination is the most common and effective method for producing water. However, it cannot be used in areas that do not have access to sea or saline water because it requires a significant amount of saline or brackish water. Desalination plants and long pipelines, on the other hand, necessitate significant capital investments. Therefore, poor and noncoastal regions, many of which suffer from chronic severe water scarcity, do not require distillation. Another potential source of potable water is the production of water in the atmosphere. There are approximately 12,900 billion tons of fresh water in the earth's atmosphere, 98% of which is vapor and the rest in a condensed state (clouds and fog), making it an enormous and renewable water resource (Inbar et al., 2020).

An atmospheric water generator, or AWG for short, is a device that turns moisture from the air into drinkable, sterile water (Siddiqui et al., 2022). To reduce a variety of chemical and biological contamination, it includes technologies for water treatment as well as filtration systems for air and water. The AWG is regarded as a promising alternative or additional source of safe drinking water, whose quality is determined by air and meteorological factors (Inbar et al., 2020). An AWG produces potable water, which is safe for human consumption.

The typical workflow for an AWG is as follows: condense the moisture that has been captured from the thin air into liquid water (Y. Tu et al., 2018). After that, the water is disinfected and filtered to ensure that it is safe for consumption by humans.

The AWG's capacity to generate water from relatively dry air and low temperatures is its most promising feature (Inbar et al., 2020). Since no conventional water source is required, AWGs offer a number of advantages over conventional water sources like wells and municipal water systems. AWGs are extremely portable, cost-effective, practical, dependable, and safe. They give you complete control over how much water you need, and there is no need to invest in expensive piping infrastructure (Mahadevan & Vairamuthu, 2020). Since atmospheric humidity is naturally renewed and the process does not harm the environment, AWG will be a renewable and sustainable water resource if the input energy comes from a clean energy source like solar, wind, biomass, or geothermal (Faraz Ahmad et al., 2022).

Although using AWGs may have advantages, there are some drawbacks. The condensation and separation processes use up energy (Y. Tu et al., 2018). Temperature, humidity, and pollution in the air all have an impact on an AWG's effectiveness. The AWG is less affected by variable abiotic conditions like sky emissivity, wind speed, and topographic location than passive condensers, despite the fact that relative humidity has a significant impact on its efficiency. As a result, it may be operable in a wider variety of weather conditions(Inbar et al., 2020).

The following research questions (RQs) are the focus of the current investigation:

RQ1. What are the current technologies and methods used in atmospheric water generators?

RQ2. What improvements and advancements can be made to atmospheric water generator technology?

RQ3. How economically and environmentally sustainable is the use of atmospheric water generator technology?

The following are the research goals that result from the aforementioned RQs:

(1) To investigate the current technology and methods used in atmospheric water generators.

(2) To identify potential improvements and advancements in atmospheric water generator technology.

(3) To study the economic and environmental sustainability of using atmospheric water generator technology.

2. Literature Review

Water vapor can be extracted from the atmosphere in a variety of ways by adjusting the system's pressure, volume, or temperature to cause condensation. Many different kinds of devices that are currently available on the market exhibit the forced natural occurrence of condensation. The condensation of air is incorporated into the design technology of air conditioners, refrigerators, and dehumidifiers. (Institute of Electrical and Electronics Engineers, n.d.).

The Atmospheric Water Generator has a lot of potential for supplying water for community use in dry areas, producing portable water using decentralized systems, and providing emergency water in times of disaster. The critical need for self-sufficiency in potable water supply through small-scale, decentralized water production in developing and impoverished regions of the world is highlighted in the United Nations' millennium development goals (Y. Tu et al., 2018).

The atmosphere provided the answer to the need for a renewable and sustainable resource to help alleviate water scarcity worldwide (Institute of Electrical and Electronics Engineers, n.d.). Innovative devices known as atmospheric water generators (AWGs) use cutting-edge technology to transform air into potable water. These machines are made to meet the rising demand for freshwater in places where there are few or contaminated traditional water sources. AWGs can help alleviate water shortages and enhance the quality of life for people living in arid or water-stressed regions due to their ability to produce water from the air.

By harvesting water from the atmosphere, which is a renewable resource, AWGs provide a sustainable solution to the water crisis. This is one of the main advantages of AWGs. This is especially important in places where there is a lot of water shortage because the machines can make water without requiring expensive and energy-intensive infrastructure. AWGs can also be used to provide water in emergency situations where traditional water sources may not be available, such as natural disasters or humanitarian crises.

AWGs can be powered by a variety of energy sources, including solar, wind, and conventional electricity, making them suitable for use in off-grid or remote locations. AWGs also require relatively little upkeep and are simple to operate. Additionally, they are portable and simple to transport to various locations.

In conclusion, atmospheric water generators are a novel approach to the problem of water scarcity that has the potential to enhance the standard of living of those who live in water-stressed areas. They are long-lasting, require little upkeep, are simple to operate, and can be moved, making them ideal for supplying clean drinking water in a variety of settings. AWGs are an important technology to think about for future research and development because of the pressing need to find long-term solutions to the water crisis and the rising demand for freshwater.

Lack of research on the systems' long-term effectiveness and efficiency in producing safe and potable water is one potential research gap in the field of atmospheric water generators (AWGs). Water is just a byproduct of AWG's use of electricity, which is not renewable (R. Tu & Hwang, 2020). While there is some research on the principles and technologies involved in AWGs, as well as short-term field tests, there is a need for more extensive testing and evaluation of these systems over an extended period of time in various climates and environments. Additionally, there is a need for research on the overall cost-effectiveness of AWGs as a water sourcing solution, including analysis of maintenance costs and energy usage. Additionally, there is a need for research on the safety and purity of water produced by these systems, as well as on the potential health effects of consuming this water over the long-term. There is a need for more extensive testing and evaluation of these systems over an extended period of time in various climates and environments, in addition to short-term field tests and research on the principles and technologies involved in AWGs. Additionally,

research on the overall cost-effectiveness of AWGs as a water-sourcing solution is required, including an examination of energy consumption and maintenance costs. Both the potential long-term health effects of consuming this water and the safety and purity of the water produced by these systems require investigation. The gaps that are worth mentioning include studies on the effect of material thickness, coating, and thermal conductivity of evaporator coils on water generation, optimization and modified design of evaporator coils, and calculations of the levelized cost of water (Raveesh et al., 2021).

3. Proposed Design

A cooling coil is utilized to condense water vapor from the air in all of the AWG designs and technologies that are utilized. Desiccants, which are substances that are capable of absorbing water vapor from the air, are used by some AWGs to cool the air while others use refrigeration. In addition, AWGs use a variety of filtration and disinfection techniques to guarantee that the produced water is safe for consumption.

3.1 Main components of the AWG:

1. Body: All of the components will be assembled in this body (Fig 1.1 and Fig. 1.2).

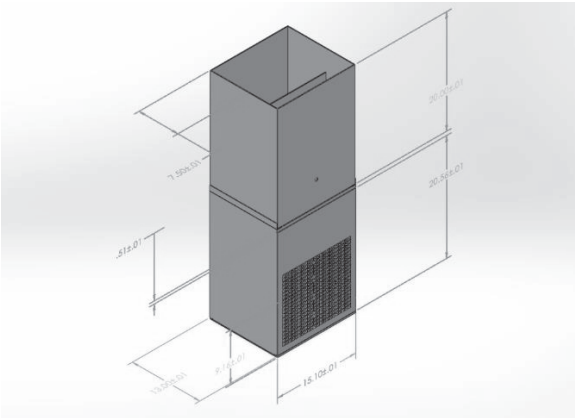

Figure 1.1: Body - Front

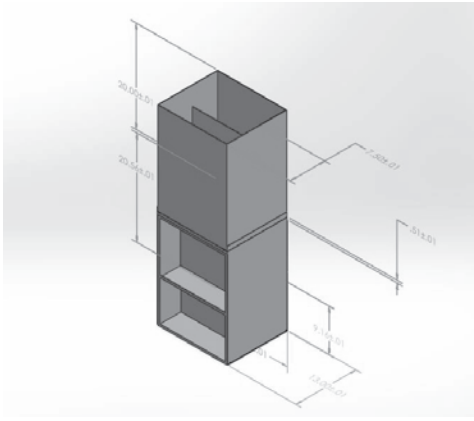

Figure 1.2: Body – Back

2. Compressor: It is a mechanical device that reduces a gas's volume to increase its pressure. A specific kind of gas compressor is an air compressor. Pumps and compressors are similar: Both can transport a fluid through a pipe and increase the pressure on the fluid. The compressor also reduces the volume of a gas because gases can be compressed. While some liquids can be compressed, they are relatively incompressible. A pump's primary function is to pressurize and transport liquids (Muhsin & Vijayan, 2022).

   The product's lower front will be the location of this component. The refrigerant is pressured to evaporate and condense by the compressor (Fig. 2).

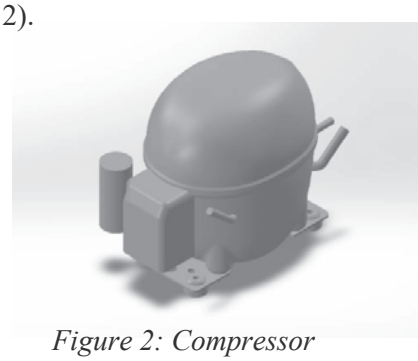

Figure 2: Compressor

3. Exhaust Air Grille: This is connected to the lower front portion of the body. The front panel exhausts the air (Fig. 3).

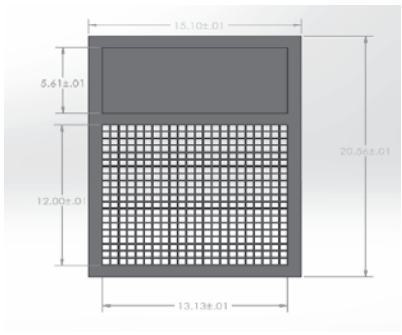

Figure 3: Exhaust Air Grille

4. Motor: In order to produce motion, electric motors convert electrical energy into mechanical energy. It generates energy that spins (Fig. 4).

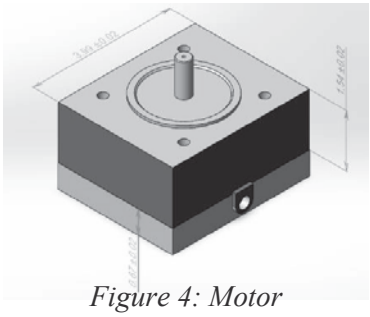

Figure 4: Motor

5. Propeller: This is connected to the motor. Moist air is drawn into the coils by the propeller (Fig. 5).

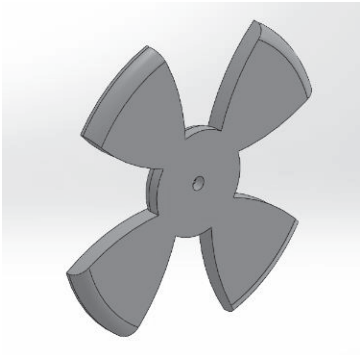

Figure 5: Propeller

6. Condenser and Evaporator: A condenser is a unit or device that is used to cool a substance from its gaseous to liquid state in systems that involve heat transfer. The substance will release the latent heat as a result, transferring it to the coolant for the condenser. Refrigerant is circulated by a compressor through a condenser and an evaporator coil to cool the air around it. Water will condense as the air temperature drops below its dew point as a result. Filtered air is pushed over the coil by a fan with a speed control (Muhsin & Vijayan, 2022; Tripathi et al., 2016). The cold coils of an evaporator (Fig. 6) remove moisture from the air.

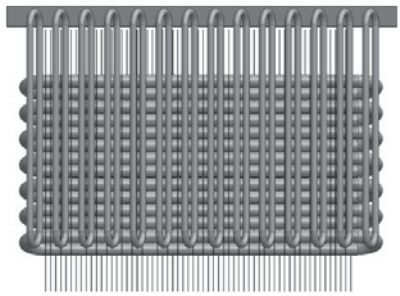

Figure 6: Condenser and Evaporator

7. HEPA Filter: The type of filter where all undesirable particulates, including dust, particulate matter, and any other particles, are eliminated(Ali et al., 2022). This is connected ahead of the evaporator. The majority of harmful particles, such as mold spores, dust, dust mites, pet dander, and other irritating allergens, are removed from the air by a HEPA (High Efficiency Particle Arresting) filter (Fig. 7).

Figure 7: High Efficiency Particle Arresting Filter

8. Water Tank: Water that was transformed from air is stored in this, which is situated at the lower back portion of the body (Fig. 8).

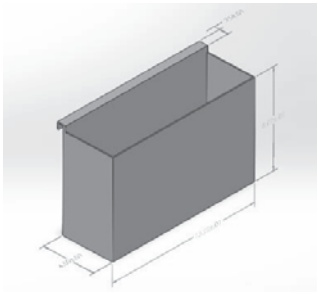

Figure 8: Water Tank

9. Water Filter: The primary benefit of gravity-based water purifiers is that they do not require electricity because water is filtered through the normal gravity process from a higher point to a lower point (Muhsin & Vijayan, 2022). Iron rust, particles, chlorine, and heavy metals are all removed from water by this filter, which is used to purify it. Ultraviolet (UV), ozone, multistage mineral, and carbon filters are just a few of the stages that go through water (Fig. 9). These stages are used to add minerals to the water and get rid of any bacteria that might be in the water (Ali et al., 2022).

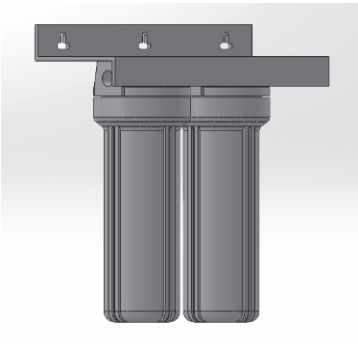

Figure 9: Water Filter

10. Water Pump: Water is pressurized, circulated, or pumped to the water filter with this pump (Fig. 10).

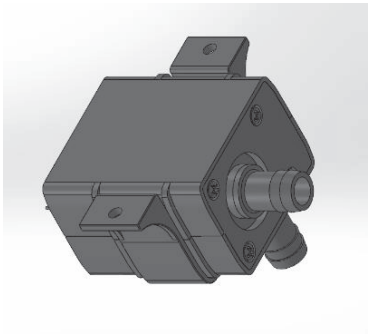

Figure 10: Water Pump

11. Holder: This component (Fig. 11) connects the upper and lower portion of the body together.

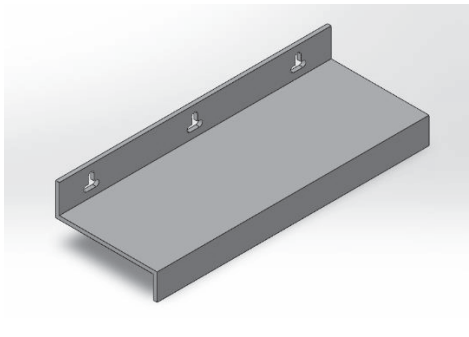

Figure 11: Holder

3.2 Final view of the proposed design:

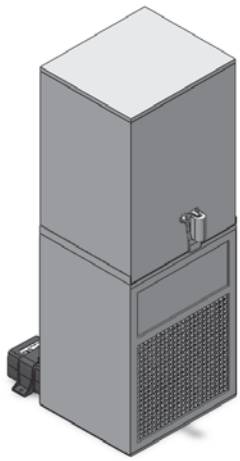

Figure 12: Final Assembled View

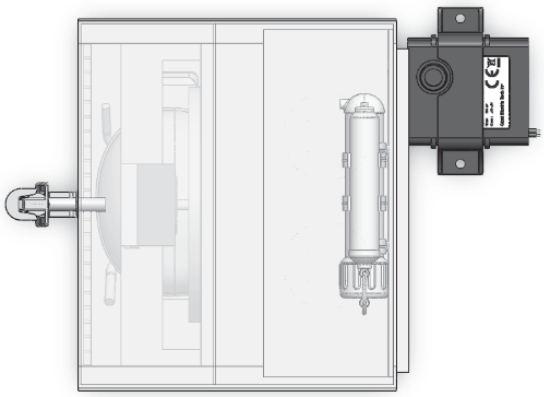

Figure 13: Top View

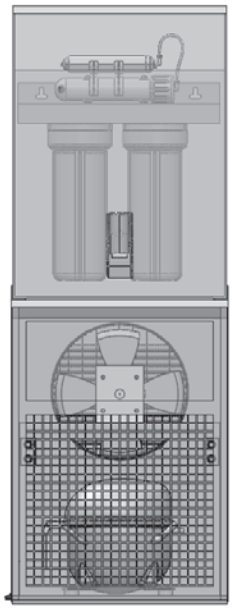

Figure 14: Front View

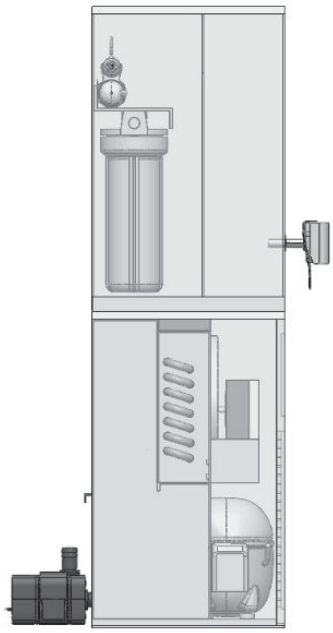

Figure 15: Left View

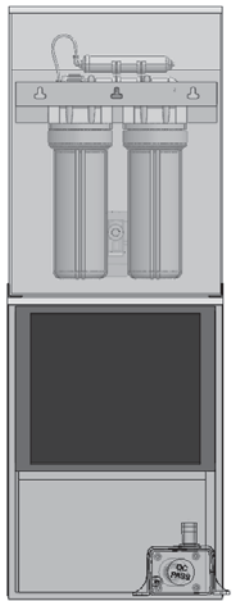

Figure 16: Back View

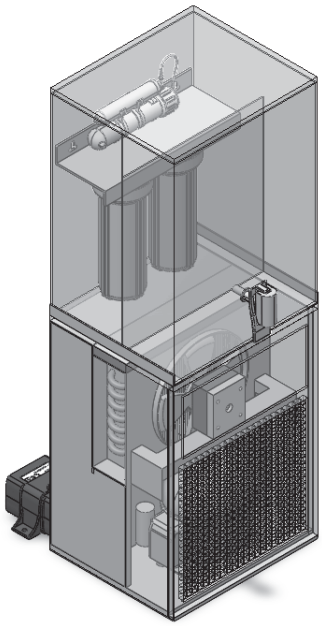

Figure 17: Isometric View

The fan and the refrigerant flow are propelled by the compressor. The high efficiency particulate air (HEPA) filter is used by the fan to move humid air through it. A series of very cold coils (evaporator) greet the filtered air. On the cold coils, the water from the air condenses. The water is collected by the water tank. Dry air is pushed out by the same fan. A 12V water pump is used to move water from the tank to the water filter through a pipe. The water is then stored in the top reservoir compartment after being filtered (Fig. 12 - Fig. 17).

3.3 Stress analysis of the components:

The stress analysis aids in determining whether the structures meet expectations and how a product can be improved. The study of stresses in materials and structures when a force is applied to them is known as stress analysis. Materials can deform or fracture under stress (Fig. 18). The goal of stress analysis is to determine how much stress causes a material to deform.

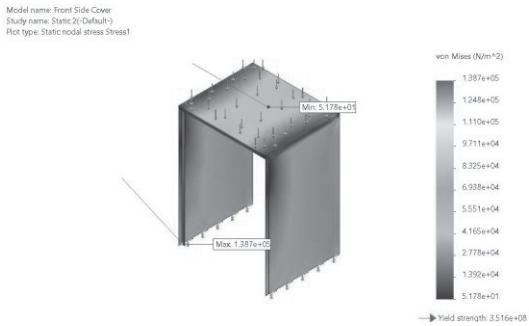

Figure 18: Stress Analysis of Lower Body Cover

The purple arrows indicate external loads (force) and the green arrows show the fixture. The dark blue color indicates medium stress all over the product body.

Breaking Range: (1.110e+05) –(1.387e+05) N/m^2

Medium Range: (5.551e+04) – (9.771e+04) N/m^2

Safe Range: (5.178e+01) – (4.165e+04) N/m^2

The Material used was Stainless Steel which has a yield strength of 206807000 N/m^2. From simulation, it was seen that the highest allowable stress that can be applied is 9.711e+04 N/m^2.

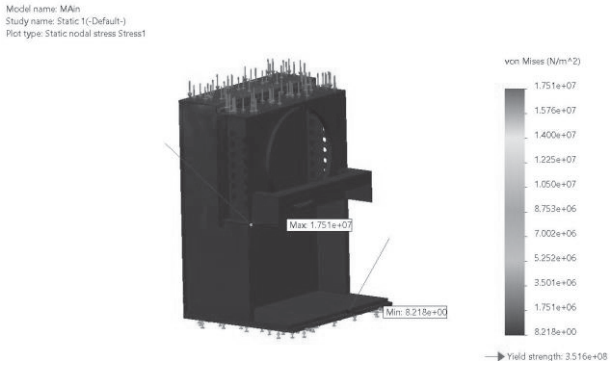

Figure 19: Stress Analysis of Lower Body Frame (Front View)

The purple arrows indicate external loads (force) and the green arrows show the fixture.

The dark blue color indicates medium stress all over the product body (Fig. 19).

Breaking Range: (1.400e+07) – (1.751e+07) N/m^2

Medium Range: (7.002e+06) – (1.225e+07) N/m^2

Safe Range: (8.218e+00) – (5.25e+06) N/m^2

The Material used was Stainless Steel which has a yield strength of 206807000 N/m^2 From simulation, it was seen that the highest allowable stress that can be applied is 1.225e+07 N/m^2 (Fig. 20).

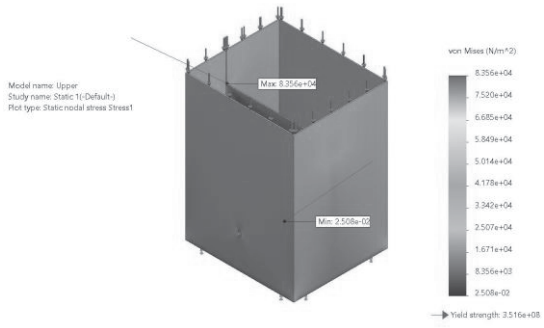

Figure 20: Stress Analysis of Filter Compartment

The purple arrows indicate external loads (force) and the green arrows show the fixture. The dark blue color indicates medium stress all over the product body.

Breaking Range: (6.685e+04) – (8.356e+04) N/m^2

Medium Range: (3.342e+04) – (5.849e+04) N/m^2

Safe Range: (2.508e-02) – (2.507e+04) N/m^2

The Material used was Stainless Steel which has a yield strength of 206807000 N/m^2 From simulation, it was seen that the highest allowable stress that can be applied is 8.356e+05 N/m^2.

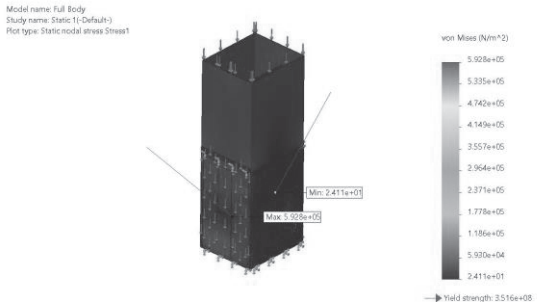

Figure 21: Stress Analysis of Main Body

The purple arrows indicate external loads (force) and the green arrows show the fixture. The dark blue color indicates medium stress all over the product body (Fig. 21).

Breaking Range: (4.742e+05) – (5.928e+05) N/m^2

Medium Range: (2.371e+05) – (4.149e+05) N/m^2

Safe Range: (2.411e+01) – (1.778e+05) N/m^2

The Material used was Stainless Steel which has a yield strength of 206807000 N/m^2 From simulation, it was seen that the highest allowable stress that can be applied is 5.928e+05 N/m^2.

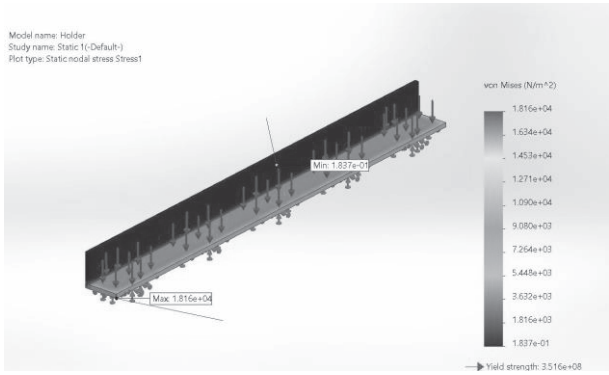

Figure 22: Stress Analysis of Angular Rail

The purple arrows indicate external loads (force) and the green arrows show the fixture. The dark blue color indicates medium stress all over the product body (Fig. 22).

Breaking Range: (1.453e+04) – (1.816e+04) N/m^2

Medium Range: (7.264e+03) – (1.271e+04) N/m^2

Safe Range: (1.837e-01) – (5.448e+03) N/m^2

The Material used was Stainless Steel which has a yield strength of 206807000 N/m^2 From simulation, it was seen that the highest allowable stress that can be applied is 1.816e+04 N/m^2.

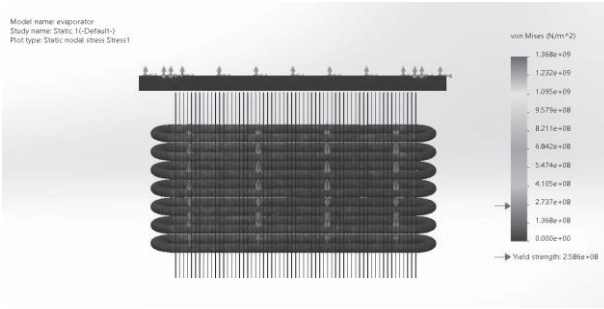

Figure 23: Stress Analysis of Copper Coil

The purple arrows indicate external loads (force) and the green arrows show the fixture (Fig. 23). The dark blue color indicates medium stress all over the product body.

Breaking Range: (1.095e+09) – (1.368e+09) N/m^2

Medium Range: (5.474e+08) – (9.579e+08) N/m^2

Safe Range: (0.000e+00) – (4.105e+08) N/m^2

Condensing pipes are made of copper (Kumar & Yadav, 2015) which has a yield strength of 258646000 N/m^2. From simulation, it was seen that the highest allowable stress that can be applied is 1.095e+09 N/m^2.

4. Conclusion

Freshwater scarcity is becoming a major global problem due to an expanding population and deteriorating environment (Qi et al., 2019). There have been a number of suggestions for overcoming this water scarcity. The generation of water from air is one such method (Siddiqui et al., 2022). By converting air into drinkable water, atmospheric water generators have the potential to address the global water crisis. Condensed water from air on long surfaces is an easy way to "create" water in remote areas, coastal areas, and other areas with high humidity but little water (He et al., 2019). AWG can provide fresh water to people in trouble in tropical seas or to garrison soldiers on a small reef as an alternative (Runze et al., 2020). In regions with consistently warm and humid weather, AWG performs best (Moghimi et al., 2021). To address the difficulties and limitations of this technology, as well as to enhance AWGs' efficiency and cost-effectiveness, additional research and development are required.

5. Reference

Ali, S., Hamad, K., & Ali, W. (2022). Water Purification in Atmospheric Water Generator. *Port-Said Engineering Research Journal*, *0*(0), 0–0. https://doi.org/10.21608/pserj.2022.134228.1180

Faraz Ahmad, F., Ghenai, C., al Bardan, M., Bourgon, M., & Shanableh, A. (2022). Performance analysis of atmospheric water generator under hot and humid climate conditions: Drinkable water production and system energy consumption. *Case Studies in Chemical and Environmental Engineering*, *6*. https://doi.org/10.1016/j.cscee.2022.100270

He, W., Yu, P., Hu, Z., Lv, S., Qin, M., & Yu, C. (2019). Experimental study and performance analysis of a portable atmospheric water generator. *Energies*, *13*(1). https://doi.org/10.3390/en13010073

Inbar, O., Gozlan, I., Ratner, S., Aviv, Y., Sirota, R., & Avisar, D. (2020). Producing safe drinking water using an atmospheric water generator (Awg) in an urban environment. *Water (Switzerland)*, *12*(10), 1–19. https://doi.org/10.3390/w12102940

Institute of Electrical and Electronics Engineers. (n.d.). *2016 IEEE Systems and*

Information Engineering Design Symposium (SIEDS) : date, 29-29 April 2016.

Kumar, M., & Yadav, A. (2015). Experimental investigation of solar powered water production from atmospheric air by using composite desiccant material "CaCl2/saw wood." *Desalination*, *367*, 216–222. https://doi.org/10.1016/j.desal.2015.04.009

Mahadevan, T. K., & Vairamuthu, S. (2020). *Development of mini Atmospheric Water Generator plant Dr.TTM,kannan View project tool design View project*. https://www.researchgate.net/publication/341990420

Mendoza-Escamilla, J. A., Hernandez-Rangel, F. J., Cruz-Alcántar, P., Saavedra-Leos, M. Z., Morales-Morales, J., Figueroa-Diaz, R. A., Valencia-Castillo, C. M., & Martinez-Lopez, F. J. (2019). A feasibility study on the use of an atmospheric water generator (AWG) for the harvesting of fresh water in a semi-arid region affected by mining pollution. *Applied Sciences (Switzerland)*, *9*(16). https://doi.org/10.3390/app9163278

Moghimi, F., Ghoddusi, H., Asiabanpour, B., & Behroozikhah, M. (2021). Is atmospheric water generation an economically viable solution? *Clean Technologies and Environmental Policy*, *23*(3), 1045–1062. https://doi.org/10.1007/s10098-020-02015-6

Muhsin, M. T., & Vijayan, A. C. (2022). Atmospheric Water Generator. In *International Journal of Research in Engineering and Science (IJRES) ISSN* (Vol. 10). www.ijres.org

Qi, H., Wei, T., Zhao, W., Zhu, B., Liu, G., Wang, P., Lin, Z., Wang, X., Li, X., Zhang, X., & Zhu, J. (2019). An Interfacial Solar-Driven Atmospheric Water Generator Based on a Liquid Sorbent with Simultaneous Adsorption–Desorption. *Advanced Materials*, *31*(43). https://doi.org/10.1002/adma.201903378

Raveesh, G., Goyal, R., & Tyagi, S. K. (2021). Advances in atmospheric water generation technologies. In *Energy Conversion and Management* (Vol. 239). Elsevier Ltd. https://doi.org/10.1016/j.enconman.2021.114226

Runze, D., Qingfen, M., Hui, L., Gaoping, W., Wei, Y., Guangfu, C., & Yifan, C. (2020). Experimental investigations on a portable atmospheric water generator for maritime rescue. *Journal of Water Reuse and Desalination*, *10*(1), 30–44. https://doi.org/10.2166/WRD.2020.048

Siddiqui, M. A., Azam, M. A., Khan, M. M., Iqbal, S., Khan, M. U., & Raffat, Y. (2022). Current trends on extraction of water from air: an alternative solution to water supply. In *International Journal of Environmental Science and Technology*. Springer Science and Business Media Deutschland GmbH. https://doi.org/10.1007/s13762-022-03965-8

Tripathi, A., Tushar, S., Pal, S., Lodh, S., Tiwari, S., & Desai, R. S. (2016). Atmospheric Water Generator. In *International Journal of Enhanced Research in Science* (Vol. 5).

Tu, R., & Hwang, Y. (2020). Reviews of atmospheric water harvesting technologies. In *Energy* (Vol. 201). Elsevier Ltd. https://doi.org/10.1016/j.energy.2020.117630

Tu, Y., Wang, R., Zhang, Y., & Wang, J. (2018). Progress and Expectation of Atmospheric Water Harvesting. In *Joule* (Vol. 2, Issue 8, pp. 1452–1475). Cell Press. https://doi.org/10.1016/j.joule.2018.07.015

Design and Development of a Battery Powered Motor Driven Rice Transplanting Machine

Mohammad Harun-Or-Rashid[1], Sabrina Alam Rasha[2], Shafkat Emran[2], Abrar Jahin Haider[2], Shahanaz Begum[3]
Department of Mechanical and Production Engineering (MPE)
[1,2]Ahsanullah University of Science and Technology (AUST), Tejgaon, Dhaka 1208, Bangladesh
[3]Department of Agricultural Extension, Khamarbari, Farmgate, Dhaka
Corresponding Email: harun.mpe@aust.edu, harun_edu@yahoo.com

Abstract: ***Design and development of a Lithium battery powered motor driven low cost rice transplanting machine is discussed in this paper. Mechanical design of the machine was done in SolidWorks. After completion of the design phase different components of the transplanting machine were manufactured and assembled. An industrial grade plant picker is attached with the motor through a chain and rotational mechanism. A lead screw mechanism was employed to move the plant tray precisely along the machine's longitudinal axis. A electric motor of one horse power was used to operate the picker. The machine's and the plant picker's speed were controlled by using an accelerator, that is, the number of rice plant transplanting per minute can be managed through the accelerator.***

Keywords: Agriculture, Lead screw *mechanism; Rice transplanting machine; rice picker.*

INTRODUCTION

Agriculture is a vital sector for the application of new technologies. These days' robotics science and engineering is transforming to agricultural sector which reduces the manpower and cost. On the other hand, increases the productivity. This paper explores the potential of agricultural robotics, considers its possible effects.

An automated planting machine is introduced by Mohammed Amer et al. [1] which is proposed to increase the speed and precision of planting. They focused on the distance between each two neighbor seedlings during plantation. An automatic seedling transplanter based on embedded system was developed by Abhijit Khadatkar et al. [2]. According to Singh, et al. [3] manual rice transplanting is a boring and time consuming operation require about 250 to 300 man hours per hectare. It means that huge manpower is needed in agricultural sector for planting paddy plants. On the other hand, rice transplanting issues, technological limitations as well as future research to build more useful mechanical transplanter is presented in the research paper of Hafijur Rahaman et al. [4]. Design of a laboratory scale seeder is proposed by A. A. Sani et al. [5]. N. R. Bhardwaj et al. developed an Arduino based robot for disease detection of plants through image processing [6]. Adoption of the mechanical rice transplanting machine is discussed by A. K. M. Saiful Islam et al. [7].

Bangladesh being an agricultural land generates huge revenue every year in the agricultural section. In 2020, contribution of agriculture on gross domestic product (GDP) is around 12% and employment in agriculture is around 38%. Therefore, huge manpower is working in this area. As a result, huge working hours are employed in this sector. If automation is implemented in this area then massive working hour can be saved as well as productivity can be increased. Since there is lack of research in automation in agricultural field of Bangladesh therefore this research is carried out. In the present study, an electric machine is introduced which is capable of rice transplant.

Design and construction of a battery powered motor driven rice transplanting machine is presented in this paper.

METHODOLOGY

First of all, in this research field observation and literature review is done. From observation it is found that there are lacks of manual as well as engine driven rice transplanting machine in Bangladesh. After literature review SolidWorks design is completed, calculation of different rotational components is done and material is selected. Then components are manufactured and assembled. A 3D model of the transplanting machine is presented in Fig. 1. Finally, experiment is conducted.

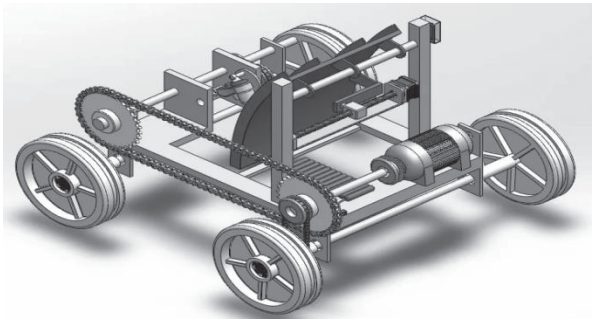

(a)

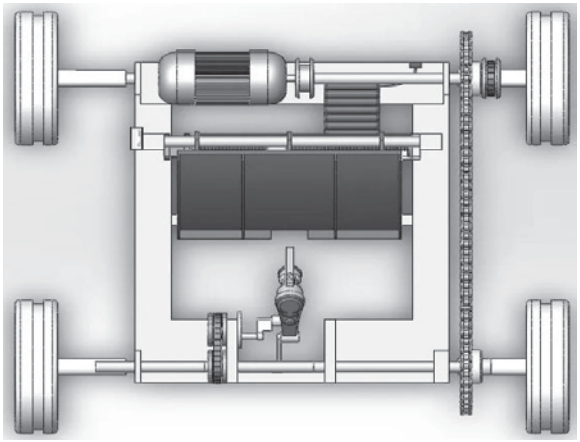

(b)

Fig. 1: Transplanting machine: (a) Right-side view, (b) Top view.

Required torque to move wheel is solved using the Eq. (1):

$$\tau = F * r \qquad (1)$$

Here, F is the force required to move on each wheel ($Mg*\mu/4$) and r is the radius of the wheel. μ is the frictional coefficient. Mass (M) of the machine is 35 Kg. Required power for each motor is presented in Eq. (2).

$$p = \omega * \tau \qquad (2)$$

Here, ω is the angular velocity of the wheel.

EXPERIMENTAL SETUP

Different components (mechanical and electrical) of the experimental setup are described in this section.

Mechanical Components

Rice picker is one of the most important among the components of the transplanter. An industrial grade rice picker is shown in Fig. 2. An electric motor transmits rotational motor through chain and sprocket mechanism to the picker. Enough torque is generated plants are picked by the trigger mechanism from the tray and push them to the ground with sufficient force.

The most important factor was to choose a tire which would be capable to drive on a muddy surface without getting stuck. Through a shaft mechanism, the motor provided the motion to the wheel. Wheel diameter is 10 inches. The two front wheels as well as the rice picker both are driven simultaneously by the 1 HP motor. With the use of an accelerator, the wheel's speed can be changed. It is important to mention that more study

Fig. 2: Rice picker

on wheel tire tread, tread shape and diameter are needed to move in muddy condition.

To transmit power from motor to the wheels and the rice picker chain is used because it can transmit more power than the belt and low maintenance cost. On the other hand, a tray is attached with the lead screw mechanism to move the tray backward and forward.

Electrical components

High energy density, fast discharge, and lengthy lifespan are the properties of Lithium Ion battery (LIB). Furthermore, LIB is used in electric vehicles and can be utilized to store solar energy. Therefore, LIB is selected in this study. A cost-effective 48v battery (Fig. 3) was built for the machine. The entire machine received 10A of current from it, which was than enough to allow for uninterrupted operation. A charger is used to charge the battery if necessary.

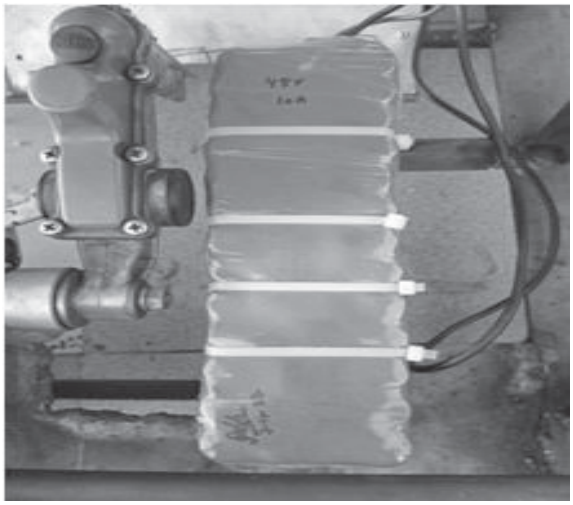

Fig. 3: Lithium Ion battery (LIB).

The main motive of electric motor is to transform electrical energy into mechanical energy. The motor supplies power to the front wheels as well as the rice picker and helps to propel the machine forward and transplant it on the ground. A one horse power motor is utilized in this study which is shown in Fig. 4.

Fig. 4: One horse power electric motor

Circuit diagram of energy transmission in presented in Fig. 5. The Lithium battery supplies energy to the motor, which then turns the front wheel shaft and rice picker. The machine begins to move forward as the front wheel begins to turn. The force of the picker's tip pushing the rice into the ground. machine's speed is adjusted with an accelerator which also helps the machine to keep an uniform speed throughout the operation.

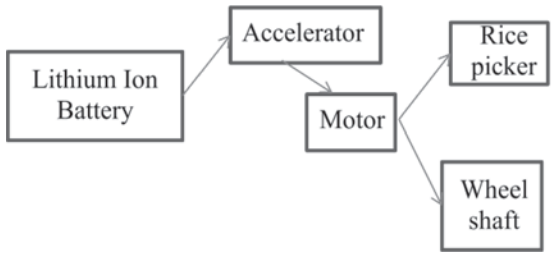

Fig. 5: Circuit diagram

The fabricated transplanting machine is shown in Fig. 6. A solar panel is attached at the top of the machine. But it is not using yet. There is a plan to run the system using electricity from the solar panel in near future.

RESULT AND DISCUSSION

From experiment it is found that, if the transplanter moves at 0.5 m/s then it can plant one rice plant in every 15.24cm. On the other hand, if, if the

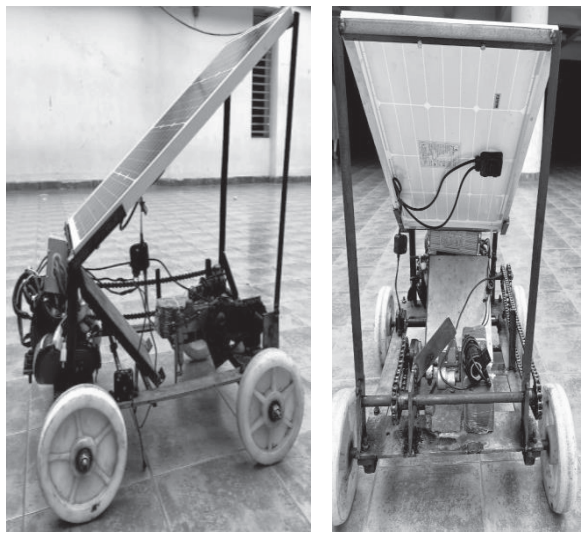

(a) (b)

Fig. 6 (a), (b): Side and back view of the rice transplanting machine (Manufactured)

transplanter moves at 1.0 m/s then it can plant one rice plant in every 10.16cm. Since the distance between two plants is normally from 15 cm to 30 cm (depend on soil quality and water) therefore 0.5 m/s velocity can be selected.

CONCLUSION

In the present study, a low cost (manufacturing cost around 60,000 taka) rice transplanting machine is designed and developed. The advantage of this transplanter is: it can moves at different speed and therefore, it is possible to adjust spacing between

plants. Further modification like making an automatic system can save huge manpower.

ACKNOWLEDGEMENT

The author would like to thank Ahsanullah University of Science and Technology (AUST), Dhaka, Bangladesh.

REFERENCES

1. M. Amer, A. Yahya, A. Daraghmeh, R. Dwaikat, and B. Nouri, Design and Development of an Automatic Controlled Planting Machine for Agriculture in Palestine, Universal Journal of Control and Automation, vol. 8, no. 2, pp. 32–39, Jun. 2020, doi: 10.13189/ujca.2020.080202.

2. Abhijit Khadatkar et al., Development of embedded automatic transplanting system in seedling transplanters for precision agriculture, Artificial Intelligence in Agriculture, Volume 5, 2021, Pages 175-184, https://doi.org/10.1016/j.aiia.2021.08.001.

3. K. N. Dewangan, Thomas and Ghosh, Performance Evaluation of a Laboratory Model Rice Technology, Agricultural Engineering Today, Vol 29, 2005.

4. H. Rahaman, Md. M. Rahman, A. K. M. S. Islam, Md. D. Huda, and M. Kamruzzaman, Mechanical Rice Transplanting in Bangladesh: Current Situation, Technical Challenges, and Future Approach, Journal of Biosystems Engineering, Oct. 2022, doi: 10.1007/s42853-022-00161-x.

5. A. A. Sani, Iskandar, D. Seprianto, R. Wilza, and R. Pradiga, Design of Automatic Rice Seeder in Laboratory Scale, in Journal of Physics: Conference Series, Mar. 2019, vol. 1167, no. 1. doi: 10.1088/1742-6596/1167/1/012059.

6. N. R. Bhardwaj, Monish R., Sunil D. M., Design and Development of an Agricultural Robot for Disease Detection in Plants and Automated Agriculture, Int J Sci Eng Res, vol. 11, no. 5, 2020.

7. A. K. M. Saiful Islam, M. T. Islam, M. A. Rabbani, M. A. Rahman, and A. B. M. Ziaur Rahman, Commercial mechanical rice transplanting under public private partnership in Bangladesh, Journal of Bioscience and Agriculture Research, vol. 6, no. 1, pp. 501–511, 2015, doi: 10.18801/jbar.060115.60.

8. Y. Vilas Deshmukh, V. Sudhir Ghodke, Y. Bharat Deore, A. Netake, A Review paper on Design and Implementation of Agriculture Robot, JARIIE-ISSN(O)-2395-4396, Vol-8 Issue-2 2022.

9. V. Kumar, H. Babu, and M. Reddy, Self-propelled Walking Behind Type Rice Transplanter-A Better Alternative For Manual Transplanting, The Andhra Agric. J 59(4): 630-634, 2012.

10. Masood Ul Hassan, M. Ullah, J. Iqbal, Towards autonomy in agriculture: Design and prototyping of a robotic vehicle with seed selector, 2nd International Conference on Robotics and Artificial Intelligence (ICRAI), 2016.

Design and Development of a Stair Climbing Four-Wheeled Robot

Mohammad Harun-Or-Rashid, Sanjida Haque, Abir Ahsan, Muhammad Sharifuzzaman Soykot
Department of Mechanical and Production Engineering (MPE)
Ahsanullah University of Science and Technology (AUST), Tejgaon, Dhaka 1208, Bangladesh
Corresponding Email: harun.mpe@aust.edu, harun_edu@yahoo.com

Abstract: ***In this paper, a stair climbing robot has been approached as well as design and development of the robot has been discussed. The four-wheeled robot which can run on a plane surface and climb stairs. The motive of this project is to build a robot which can climb through the stairs with specific load. Market survey has also been done for cost analysis. Mechanical designs were made with specific measurements. After manufacturing the mechanical components and purchasing electrical components system had been assembled according to the SolidWorks design and the circuit diagram. After several experiment on different power sources, it was decided to use 12V 30A AC to DC Switch Mode Power Supply (SMPS) and decided to use wind shield wiper motor. The setup is capable of working with very little impact on the environment.***

Keywords: *Four-wheeled robot, Motor driver (BTS-7960), Tie-rod mechanism, Wiper motor.*

1. INTRODUCTION

Robotics research has been a long tradition to overcome obstacles in human life. Technological advances become a necessity for the human being. For decades, most of the popular ideas in modern technology are how to reduce human precession from both practical and theoretical applications. Recent development has revealed that robotics has been emerged with human lives.

In recent years, there has been observed a growing interest in the mobile robotics area. A lot of research concentrates on the description of kinematic models of mobile robots and designing feedback control laws for nonholonomic systems. Researchers typically consider wheeled platforms with nonholonomic constraints white assuming perfect rolling. An excellent overview concerning different types of these robots can be found in [1].

Jonghun Choe and Ukjin Kwon (2017) alluded that, the challenge of stair climbing robot is to climb with various stair dimension [2]. Adding length adjustable mechanism, they found successful outcome to overcome the challenge. They added a tusk in front of four-wheel robot and used augmented system to detect stair dimension. Eich et al. (2008) have studied with 'ASGUARD' robot which was a hybrid legged-wheeled crawler-type that was used in a sluggish outdoor environment with a view to on security and outdoor surveillance as well as on disaster mitigation missions. A robot must to transport a variety of mission-depending application sensors inside a rough terrain to gain a successful operation. These missions were commonly named as "Three D missions", which means: dull, dirty, and dangerous [3].

In the paper of Jigar J. Parmar et, al (2014), they have discussed about the wheel which they have used in a robotic competition and it was omni wheel at angle of 45 degree [4].

As the world is moving toward robotics, research topic has been chosen in this field**.** The topic that has been chosen is **"**Design and development of a stair climbing four**-**wheeled robot**"**. This research constitutes a relative area which has emerged from Mars Rover**.** In the past two decades, design and development of mars rovers have played an important role to modern science and technology**.** This has been widely adopted in the field of robotics**.** This project closely follows the paradigm of Mars Rover. The steps were to design an effective four**-**wheeled stair climbing robot with fabrication and test the newly designed robot and investigate the experimental behavior and to conduct the performance analysis**.**

2. METHODOLOGY

Over the past few years, the scientists have tried to develop robots that can move on rough terrains**.** However, there are few robots that are suitable for use in rough terrains**.** A number of new technologies have evolved for reliable localization, obstacle avoidance and even autonomous map building in dynamically changing environment. However, mobility in very rough land is often very limited due to the absence of adequate locomotion concepts. The aim of this project is to introduce a new class of locomotive concept that will have excellent off**-**road capabilities. As a first prototype of this class, this four**-**wheeled robot will have the capability of climbing the stairs of height equal to its diameter. It

will possess maximum gripping capacity and stability during motion in rough terrain owing to the four differential driven wheel configurations**.** In the course of the experiment, other thesis works about this certain topic played an important role. After literature study and getting some knowledge about the project of four-wheeled robot and its specification the idea has been captured of how to climb the stairs**.**

The steps of the design and development process are given below:

Understand the Problem,
Identify the known and unknown parameters,
State all assumptions and decisions,
Identify and analyze the problem,
Present the solution.

After reading numerous research papers, books and watching videos an idea of a proper design of the robot was obtained.
During identification of known and unknown parameters (like dimensions, wheel radius, motor RPM, climbing speed, weight of the system, material selection, costing etc) light weight (as less as possible), knowledge of literature review and market survey are considered.
The problems have been found like the situations where the robot is not working properly and some of them are tried to solve with alternate solutions.

3. MATHEMATICAL FORMULATION

Before purchasing components, it is needed to justify which will be suitable for the desired project. For this reason, calculation plays a vital role. Among all of the components, picking out the suitable motor is most important as there is a relation between toque and force. Motor is subjected to provide the torque. After calculation of torque and rpm, motor having required specification can be known. And therefore, governing equations of torque and power are presented below.

Calculation of Torque

Total Mass of the robot with applied load on it is 40 Kg. Diameter of wheel is 0.3048 m. For selection of motor, consideration of torque has been taken. The 'torque', provided by the selected motor must be greater than the maximum torque needed for the robot during its dynamism. Required torque to move wheel is solved using the Eq. (1):

$$\tau = F * r \qquad (1)$$

Here, F is the force required to move on each wheel ($mg*\mu/4$). .Here, μ is the frictional coefficient and m is the mass of the machine. Four wheels are being used. Total torque is divided uniformly into four wheels. Estimated torque of one motor is 21.24 N-m. Hence, each motor needs to provide 21.24 N-m or more torque to move the system. Each wiper motor gives torque more than this required value. Therefore, wiper motors are selected.

Calculation of Power

In the present study, it is assumed that, load is uniformly distributed. Now, it is going to be checked out how much power is required for each wheel at different velocity (v) of the robot. Required power for each motor is presented in Eq. (2).

$$p = \omega * \tau \qquad (2)$$

Here, ω (v/r) is the angular velocity of the wheel. If the robot moves at 0.15m/s the required power for each wheel is 20.9 watt.
Free body diagram of the robot moving on ground and inclined surface are presented in Fig. 1 and Fig. 2 respectively.

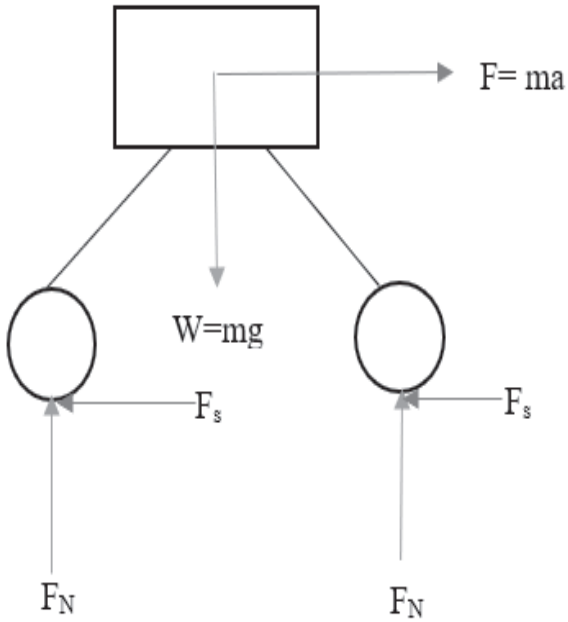

Fig. 1: Free Body diagram of the robot moving in ground surface

Here, F_N is the reaction force that acting on the wheels and Fs ($=\mu \times F$) is the friction force acting against the robot's moving direction.

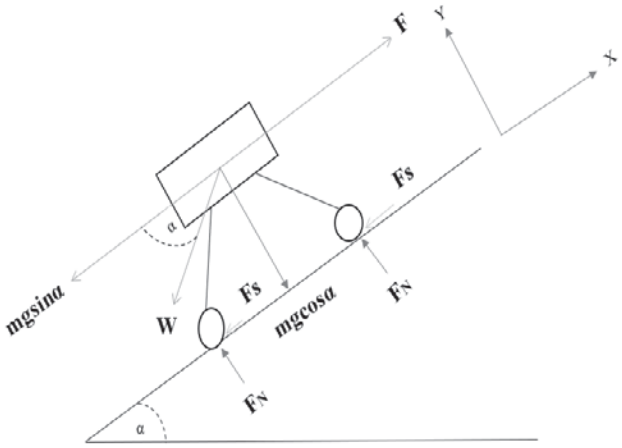

Fig. 2: Free body diagram of a climbing robot with inclined plane with friction

4. EXPERIMENTAL SETUP

Mechanical Design

First of all literature is studied and then a 3D model is designed in SolidWorks. 3D model of the robot is shown in Fig. 3.

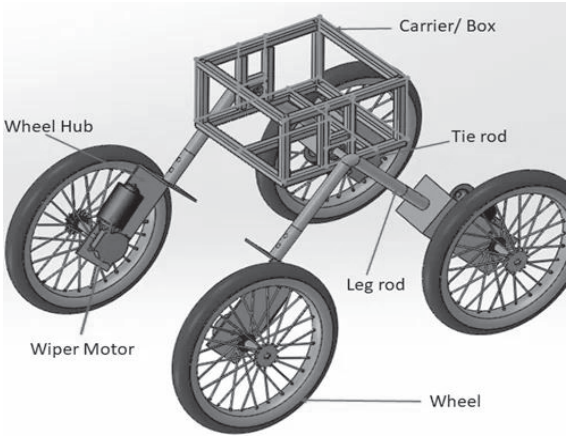

Fig. 3: SolidWorks Design (Isometric View)

Fig. 4: Tie Rod

Tie rods (Fig. 4) are used in many vehicles to connect the steering gear and knuckle in order to prevent tear in vehicle so that the vehicle can handle properly. The tie rod is used here to convert the rotary motion to linear motion so that the robot can steer.

During manufacture of the robot, a box is made according to dimension.

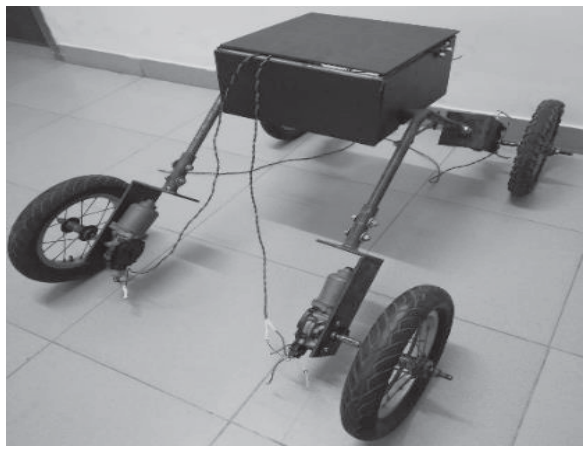

Fig. 5: Four-wheeled robot (Manufactured)

After that, two bearings are set and two bent leg rods are added trough shafts and bearing so that these can rotate freely. On the bottom part of the frame, a small ball bearing is attached which will hold a plate**.** The plate is used to hold the tie rod and helps to make movements of the robot**.** The tie rod will convert the rotary motion of the ball bearing to linear motion so that the robot can move in rocky surface and can climb stair. One side of the tie rod is connected on bottom part of the extra portion which came out from bent joint**.** Another side of tie rod is connected with the plate**. T**he wheels are attached to the hub with the help of nut-bolt**.** The wheels are jointed properly and do not create huge friction**.**

Electrical Components

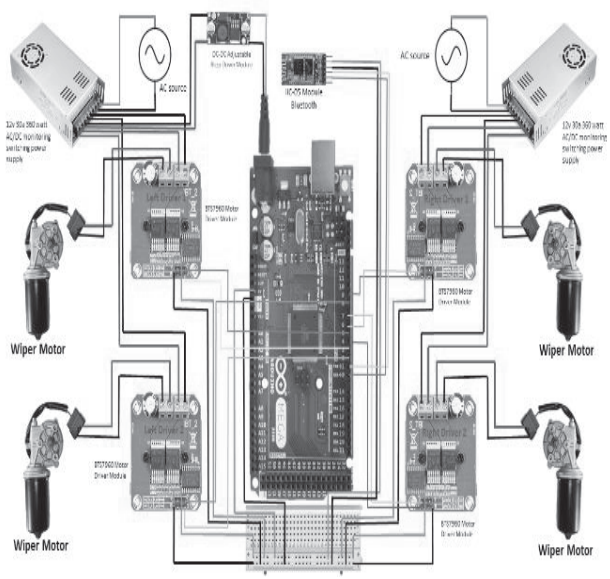

Fig. 6: Circuit Design of electrical components for four-wheeled stair climbing robot

Circuit diagram of the stair climbing robot is presented in Fig. 6. Four motor drivers (BTS7960) are used. On the other hand an Arduino Mega-2560 R3 is used as microcontroller. Each motor is connected with the motor driver and two 12V 30A power supply systems are used as power source. A Bluetooth module is connected with the microcontroller to control the robot.

5. RESULT AND DISSCUSSION

Simulation

Structural stress analysis has been done in Solid Edge (version 21) with a view to observing how much stress can be generated with given load and how much displacement can be occur on the robot. Also, from simulation, it can be known that in which location the highest stress can be generate. This study has been done only on the legs of the robot.

Materials Property

Mild steel was used to make the entire body of the robot. The simulation was run with the material steel as this option was the closest with mild steel. Material properties are given in Table 1.

Table 1: Material Property Table

Property Name	Value
Density	7833 kg/m^3
Thermal Conductivity	0.032 kW/m-C
Specific heat	481 J/kg-C
Modulus of Elasticity	199947.953 MPa
Poisson's ratio	0.29
Yield Stress	262.001 MPa
Ultimate Stress	358.527Mpa

Boundary Condition

The stress simulation was run with the leg of the robot. The load was applied in the extension part of the leg that goes inside the frame and carries the frame. The force was applied in the negative Z direction as the direction of the weight and gravity. The gravity was also considered. The pipes which go inside the wheel were constrained with pinned condition (Fig 7).

Mesh Convergence Study

In this stress simulation study, a mesh convergence study was done to find the best mesh size for the FEA model. Von Mises stress and Displacement of the model were plotted against number of elements (Fig. 8). The Solid Edge provides 10 defaults mesh sizes

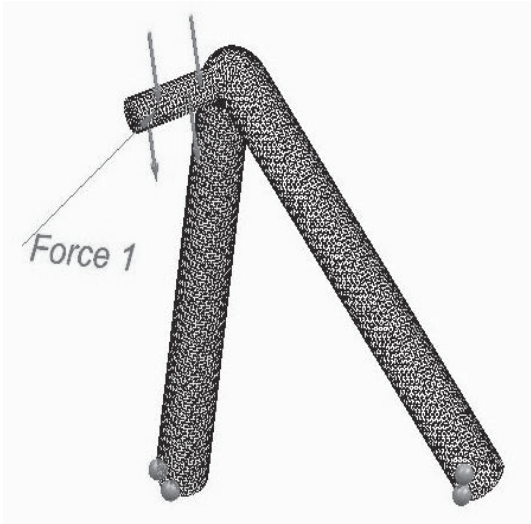

Fig. 7: Applied force and fixed points of the leg.

appropriate for the solid model. For each mesh size Von Mises stress and displacement were simulated with a constant boundary condition.

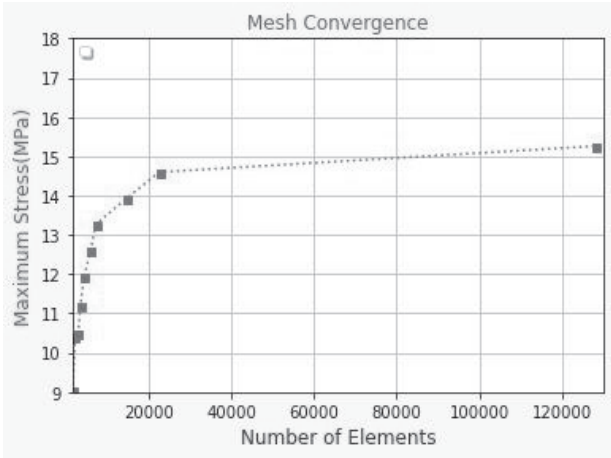

Fig. 8: Von Mises Stress versus Mesh Size

Applying five different loads, maximum stress and displacement against those have been gotten and shown in Table 2 and Fig. 9.

Table 2: Maximum stress to applied load

Applied Load (mN)	Maximum Stress (MPa)
98000	4.71
196000	9.9
294000	14.8
392000	19.8
490000	24.7

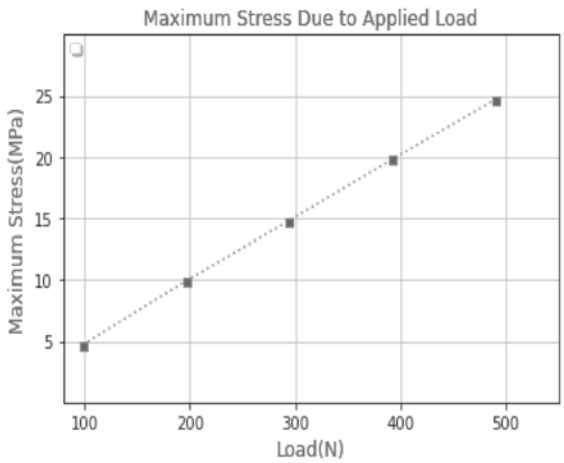

Fig. 9: Load versus maximum stress graph

In Fig. 9, for better visualization the unit of load has converted into Newton. Here, five different loads have been applied from 10 kg to 50 kg with an increment of 10 kg. This unit of 'kg' has been converted into mN in table and 'N' in graph. From the graph, it can easily be seen that with the increase of applied load, the maximum stress is also increasing. Maximum stress becomes highest, when applied load is highest. The graph is linear. The maximum stress is 24.7MPa, when the applied load is 490000 mN or 50 kg.

The wiper motor provides the torque. Compared to other motors wiper motor has much advantages for its unique performance of producing huge amount of torque. The only disadvantage is its weight. It is heavier compared to dc gear motor. Eventually, considering performance, cost and suitability it has been decided to stick with wiper motor. Lead acid batteries have been tried. But, due to low current supply, the idea of using lead acid battery has been eliminated. Instead of lead acid battery, two 12V 30A electrical power supply systems have been used to run the robot.

6. CONCLUTION

In this research, a four-wheeled stair climbing robot has been developed. At first 3D model has been designed in SolidWorks software. After design in SolidWorks, the design is taken for simulation and it has been done in Solid Edge. Then required components manufactured for constructing the robot. Then mechanical structure of the robot has been assembled. Then electrical connections have been done. Hopping to a get huge torque from motor, wiper motor has been come into consideration comparing with all type of motors. To get well-structured frame for robot body, mild steel has been used. Its lower cost is also a reason to select it. From this experience of this research it is suggested not to choose BTS motor driver as a driving module for those who want to develop similar kind of robot. A motor driver having better performance will be highly recommended. Cytron motor driver can be experimented if economical ability permits. Four different types of power supply have been experienced. Lastly, the switched mode power supply has been used in this project and better performance has been found.

7. REFERENCES

1. K. Kozłowski and D. Pazderski, MODELING AND CONTROL OF A 4-WHEEL SKID-STEERING MOBILE ROBOT, Int. J. Appl. Math. Comput. Sci., 2004, Vol. 14, No. 4. 477-496.
2. C. Jonghun, U. Kwon, M. C. Nah, and H. Kim, Design Analysis of TuskBot: Universal Stair Climbing 4-Wheel Indoor Robot, IEEE/RSJ International Conference on Intelligent Robots and Systems (IROS), 2017, doi: 10.0/Linux-x86_64.
3. M. Eich, F. Grimminger, S. Bosse, D. Spenneberg, and F. Kirchner, Asguard: A Hybrid-Wheel Security and SAR-Robot Using Bio-Inspired Locomotion for Rough Terrain, German Research Center for Artificial Intelligence (DFKI), 28359 Bremen, Germany.
4. Parmar, Jigar J., and Chirag V. Savant, Selection of wheels in robotics, Int. J. Scientific & Enginering Research, Vol. 5, Issue 10, 339-343, 2014.
5. M. A. H. Nafis, A. Chowdhury, R. I. Linda, and S. Akhtar, Design and Manufacturing of a Stair Climbing Vehicle, Proceedings of the 2010 International Conference on Industrial Engineering and Operations Management Dhaka, Bangladesh, January 9 – 10, 2010.
6. K. Kikuchi, K. Sakaguchi, T. Sudo, N. Bushida, Y. Chiba, and Y. Asai, A study on a wheel-based stair-climbing robot with a hopping mechanism, Mechanical Systems and Signal Processing, vol. 22, Issue 6, p. 1316–1326, Aug. 2008, doi: 10.1016/j.ymssp.2008.03.002.

MECHANICAL ENGINEERING DIVISION

THE INSTITUTION OF ENGINEERS, BANGLADESH

Headquarters : Ramna, Dhaka-1000, Bangladesh

Tel : 880-2-9573343, 9556112, 9559485, Fax : 880-2-9562447

E-mail : info@iebbd.org, info.iebhq@gmail.com

Design & printed by ‖ *Vivid* ‖ 01819298544